Integrase-RNA interactions underscore the critical role of integrase in HIV-1 virion morphogenesis

Short title: Key role for HIV-1 integrase-RNA interactions in virion maturation

Jennifer Elliott[1], Jenna E. Eschbach[1], Pratibha C. Koneru[2], Wen Li[3,4], Maritza Puray Chavez[1], Dana Townsend[1], Dana Lawson[1], Alan N. Engelman[3,4], Mamuka Kvaratskhelia[2], Sebla B. Kutluay[1]

[1] Department of Molecular Microbiology, Washington University School of Medicine, Saint Louis, MO 63110, USA

[2] Division of Infectious Diseases, University of Colorado School of Medicine, Aurora, CO 80045

[3] Department of Cancer Immunology and Virology, Dana-Farber Cancer Institute, Boston, MA 02215

[4] Department of Medicine, Harvard Medical School, Boston, MA 02115

Correspondence: kutluay@wustl.edu

ABSTRACT

A large number of HIV-1 integrase (IN) alterations, referred to as class II substitutions, exhibit pleotropic effects during virus replication. However, the underlying mechanism for the class II phenotype is not known. Here we demonstrate that all tested class II IN substitutions compromised IN-RNA binding in virions by one of three distinct mechanisms: i) markedly reducing IN levels thus precluding formation of IN complexes with viral RNA; ii) adversely affecting functional IN multimerization and consequently impairing IN binding to viral RNA; iii) directly compromising IN-RNA interactions without substantially affecting IN levels or functional IN multimerization. Inhibition of IN-RNA interactions resulted in mislocalization of the viral ribonucleoprotein complexes outside the capsid lattice, which led to premature degradation of the viral genome and IN in target cells. Collectively, our studies uncover causal mechanisms for the class II phenotype and highlight an essential role of IN-RNA interactions for accurate virion maturation.

INTRODUCTION

Infectious HIV-1 virions are formed in a multistep process coordinated by interactions between the HIV-1 Gag and Gag-Pol polyproteins, and the viral RNA (vRNA) genome. At the plasma membrane of an infected cell, Gag and Gag-Pol molecules assemble around a vRNA dimer and bud from the cell as a spherical immature virion, in which the Gag proteins are radially arranged [1-3]. As the immature virion buds, the viral protease enzyme is activated and cleaves Gag and Gag-Pol into their constituent domains triggering virion maturation [1, 2]. During maturation the cleaved nucleocapsid (NC) domain of Gag condenses with the RNA genome and *pol*-encoded viral enzymes [reverse transcriptase (RT) and integrase (IN)] inside the conical capsid lattice, composed of the cleaved capsid (CA) protein, which together form the core [1-3].

After infection of a target cell, RT in the confines of the reverse transcription complex (RTC) synthesizes linear double stranded DNA from vRNA [4]. The vDNA is subsequently imported into the nucleus, where the IN enzyme catalyzes its insertion into the host cell chromosome [5, 6]. Integration is mediated by the intasome nucleoprotein complex that consists of a multimer of IN engaging both ends of linear vDNA [7]. While the number of IN protomers required for intasome function varies across Retroviridae, single particle cryogenic electron microscopy (cryo-EM) structures of HIV-1 and Maedi-visna virus indicate that lentivirus integration proceeds via respective higher-order dodecamer and hexadecamer IN arrangements [8, 9], though a lower-order intasome comprised of an HIV-1 IN tetramer was also resolvable by cryo-EM [9].

A number of IN substitutions which specifically arrest HIV-1 replication at the integration step have been described [10]. These substitutions are grouped into class I to delineate them from a variety of other IN substitutions, which exhibit pleiotropic effects and are collectively referred to as class II substitutions [10-12]. Class II IN substitutions or deletion of entire IN impair proper particle assembly [11, 13-25], morphogenesis [11, 15, 21-23, 26-28] and reverse transcription in target cells [10, 11, 17, 19-21, 23, 25-44], in some cases without impacting IN catalytic function [15, 16, 19, 20, 30, 31, 34, 36, 45-47]. A hallmark morphological defect of these viruses is the formation of aberrant viral particles with viral ribonucleoprotein (vRNP) complexes mislocalized outside of the conical CA lattice [11, 15, 21-23, 26-28]. Strikingly similar morphological defects are observed in virions produced from cells treated with allosteric integrase inhibitors (ALLINIs, also known as LEDGINs, NCINIs, INLAIs or MINIs) [26, 27, 48-55]. ALLINIs induce aberrant IN multimerization in virions by engaging the V-shaped pocket at the IN dimer interface, which also provides a principal binding site for the host integration targeting cofactor lens epithelium-derived growth factor (LEDGF)/p75 [50, 54, 56-60]. The recent discovery that HIV-1 IN binds to the vRNA genome in virions and that inhibiting IN-RNA

77 interactions leads to the formation of eccentric particles provided initial clues about the role of IN
78 during virion morphogenesis [28].

79 HIV-1 IN consists of three independently folded protein domains: the N-terminal domain
80 (NTD), catalytic core domain (CCD), and C-terminal domain (CTD) [7, 61], and vRNA binding is
81 mediated by a constellation of basic residues within the CTD [28]. However, class II IN
82 substitutions are located throughout the entire length of the IN protein [10, 12], which raises the
83 question as to how these substitutions impair virus maturation. The structural basis for IN
84 binding to RNA is not yet known; however, in vitro evidence indicates that IN binds RNA as
85 lower-order multimers, and conversely RNA binding may prevent the formation of higher order
86 IN multimers [28]. Notably, aberrant IN multimerization underlies the inhibition of IN-RNA
87 interactions by ALLINIs [28] and subsequent defects in virion maturation [26-28, 48, 49, 51-55].
88 Therefore, it seems plausible that class II IN substitutions may exert their effect on virus
89 replication by adversely affecting functional IN multimerization. However, a systematical
90 evaluation of the effects of IN substitutions on IN multimerization, IN-RNA binding, and virion
91 morphology is lacking. As such, it remains an open question how functional IN multimerization
92 and/or IN-RNA interactions influence correct virion morphogenesis.

93 Eccentric virions generated via class II IN substitutions or ALLINI treatment are defective
94 for reverse transcription in target cells [10, 11, 17, 19-21, 23, 25-44, 48, 49, 51, 54, 58, 62]
95 despite containing equivalent levels of RT and vRNA genome as wild type (WT) particles [26,
96 63]. In addition, neither the condensation of the viral genome by NC [26, 63] nor its priming [63]
97 appear to be affected. We and others have recently shown that premature loss of the viral
98 genome and IN, as well as spatial separation of RT from vRNPs, may underlie the reverse
99 transcription defect observed in eccentric viruses generated in the presence of ALLINIs or the
100 class II IN R269A/K273A substitutions [59, 64]. These findings support a model in which the
101 capsid lattice or IN binding to vRNA itself is necessary to protect viral components from the host

environment upon entering a target cell. Whether the premature loss of the viral genome and IN is a universal outcome of other class II IN substitutions is unknown.

In this work, we aimed to determine the molecular basis of how class II IN substitutions exert their effects on HIV-1 replication. In particular, by detailed characterization of how class II substitutions impact IN multimerization, IN-RNA interactions and virion morphology, we aimed to dissect whether loss of IN binding to vRNA or aberrant IN multimerization underlies the pleiotropic defects observed in viruses bearing class II IN mutations. Remarkably, we found that class II substitutions either prevented IN binding to the vRNA genome or precluded the formation of IN-vRNA complexes through reducing or eliminating IN from virions. We show that IN tetramers have a strikingly higher affinity towards vRNA than IN monomers or dimers, and a large number of class II IN substitutions inhibited IN binding to RNA indirectly through modulating functional IN tetramerization. In contrast, R262A/R263A and R269A/K273A substitutions within the CTD and the K34A change within the NTD did not perturb IN tetramer formation, and thus likely directly interfered with IN binding to RNA. Irrespective of how IN-RNA binding was inhibited, all class II IN mutant viruses formed eccentric particles with vRNPs mislocalized outside of the CA lattice. Subsequently, this led to premature loss of the vRNA genome as well as IN, and spatial separation of RT and CA from the vRNPs in target cells. Taken together, our findings uncover causal mechanisms for the class II phenotype and highlight the essential role of IN-RNA interactions for the formation of correctly matured virions and vRNP stability in HIV-1-infected cells.

MATERIALS AND METHODS

Plasmids

The pNLGP plasmid consisting of the HIV-1_{NL4-3}-derived Gag-Pol sequence inserted into the pCR/V1 plasmid backbone [65] and the CCGW vector genome plasmid carrying a GFP reporter

under the control of the CMV promoter [66, 67] were previously described. The pLR2P-vprIN plasmid expressing a Vpr-IN fusion protein has also been previously described [68]. Mutations in the IN coding sequence were introduced into both the pNLGP plasmid and the HIV-1_{NL4-3} full-length proviral plasmid (pNL4-3) by overlap extension PCR. Briefly, forward and reverse primers containing IN mutations in the *pol* reading frame were used in PCR reactions with antisense and sense outer primers containing unique restriction endonuclease sites (AgeI-sense, NotI-antisense for NLGP and AgeI-sense, EcoRI-antisense for pNL4-3), respectively. The resulting fragments containing the desired mutations were mixed at 1:1 ratio and overlapped subsequently using the sense and antisense primer pairs. The resulting fragments were digested with the corresponding restriction endonucleases and cloned into pNLGP and pNL4-3 plasmids. IN mutations were introduced into the pLR2P-vprIN plasmid using the QuickChange Site-Directed Mutagenesis kit (Agilent Technologies). Presence of the desired mutations and absence of unwanted secondary changes were verified by Sanger sequencing.

Cells and viruses

HEK293T cells (ATCC CRL-11268) and HeLa-derived TZM-bl cells (NIH AIDS Reagent Program) were maintained in Dulbecco's modified Eagle's medium supplemented with 10% fetal bovine serum. MT-4 cells were maintained in RPMI 1640 medium supplemented with 10% fetal bovine serum. CHO K1-derived pgsA-745 cells (CRL-2242, ATCC) that lack a functional xylosyltransferase enzyme and as a result do not produce glycosaminoglycans were maintained in Dulbecco's modified Eagle's / F12 (1:1) media supplemented with 10% fetal bovine serum and 1 mM L-glutamine. Single-cycle GFP reporter viruses pseudotyped with vesicular stomatitis virus G protein (VSV-G) were produced by transfection of HEK293T cells with pNLGP-derived plasmids, the CCGW vector genome carrying GFP, and VSV-G expression plasmid at a ratio of 5:5:1, respectively, using polyethyleneimine (PolySciences, Warrington, PA). Full-length viruses pseudotyped with VSV-G were produced by transfecting HEK293T cells with the pNL4-3-derived plasmids and VSV-G plasmid at a ratio of 4:1 (pNL4-3:VSV-G).

Immunoblotting

Viral and cell lysates were resuspended in sodium dodecyl sulfate (SDS) sample buffer and separated by electrophoresis on Bolt 4-12% Bis-Tris Plus gels (Life Technologies), blotted onto nitrocellulose membranes and probed overnight at 4°C with the following antibodies in Odyssey Blocking Buffer (LI-COR): mouse monoclonal anti-HIV p24 antibody (183-H12-5C, NIH AIDS reagents), mouse monoclonal anti-HIV integrase antibody [69], rabbit polyclonal anti-HIV integrase antibody raised in-house against Q44-LKGEAMHGQVD-C56 peptide and hence unlikely to be affected by the substitutions introduced into IN in this study, rabbit polyclonal anti-HIV-1 reverse transcriptase antibody (6195, NIH AIDS reagents), rabbit polyclonal anti-Vpr antibody (11836, NIH AIDS Reagents), rabbit polyclonal anti-MA antibody (4811, NIH AIDS Reagents). Membranes were probed with fluorophore-conjugated secondary antibodies (LI-COR) and scanned using a LI-COR Odyssey system. IN and CA levels in virions were quantified using Image Studio software (LI-COR). For analysis of the fates of core components in infected cells, antibody incubations were done using 5% non-fat dry milk. Membranes were probed with HRP-conjugated secondary antibodies and developed using SuperSignal™ West Femto reagent (Thermo-Fisher).

Analysis of reverse transcription products in infected cells

MT-4 cells were grown in 24-well plates and infected with VSV-G pseudotyped pNL4-3 viruses (either WT or class II IN mutant) at a multiplicity of infection (MOI) of 2 in the presence of polybrene. Six h post-infection cells were collected, pelleted by brief centrifugation, and resuspended in PBS. DNA was extracted from cells using the DNeasy Blood and Tissue Kit (Qiagen) as per kit protocol. Quantity of HIV-1 vDNA was measured by Q-PCR using primers specific for early reverse-transcripts.

Vpr-IN transcomplementation experiments

A class I IN mutant virus (HIV-1_{NL4-3} IN_{D116N}) was trans-complemented with class II mutant IN proteins as described previously [68]. Briefly, HEK293T cells grown in 24-well plates were co-

transfected with a derivative of the full-length HIV-1_{NL4-3} proviral plasmid bearing a class I IN substitution (pNL4-3_{D116N}), VSV-G, and derivatives of the pLR2P-vprIN plasmid bearing class II IN mutations at a ratio of 6:1:3. Two days post-transfection cell-free virions were collected from cell culture supernatants. Integration capability of the trans-complemented class II IN mutants was tested by infecting MT-4 cells and measuring the yield of progeny virions in cell culture supernatants over a 6-day period as described previously [68]. In brief, MT-4 cells were incubated with virus inoculum in 96 V-bottom well plates for 4 h at 37°C after which the virus inoculum was washed away and replaced with fresh media. Immediately following removal of the virus inoculum and during the six subsequent days the quantity of virions present in the culture supernatant was quantified by measuring RT activity using a Q-PCR-based assay [70].

CLIP experiments

CLIP experiments were conducted as previously described [28, 71, 72]. Cell-free HIV-1 virions were isolated from transfected HEK293T cells. Briefly, cells in 15-cm cell culture plates were transfected with 30 μg full-length proviral plasmid (pNL4-3) DNA containing the WT sequence or indicated *pol* mutations within the IN coding sequence. Cells were grown in the presence of 4-thiouridine for 16 h prior to virus harvest. Two days post transfection cell culture supernatants were collected and filtered through 0.22 μm filters and pelleted by ultracentrifugation through a 20% sucrose cushion using a Beckman SW32-Ti rotor at 28,000 rpm for 1.5 h at 4°C. Virus pellets were resuspended in phosphate-buffered saline (PBS) and UV-crosslinked. Following lysis in RIPA buffer, IN-RNA complexes were immunoprecipitated using a mouse monoclonal anti-IN antibody [69]. Bound RNA was end-labeled with γ-^{32}P-ATP and T4 polynucleotide kinase. The isolated protein-RNA complexes were separated by SDS-PAGE, transferred to nitrocellulose membranes and exposed to autoradiography films to visualize RNA. Lysates and immunoprecipitates were also analyzed by immunoblotting using antibodies against IN.

IN multimerization in virions

HEK293T cells grown on 10-cm dishes were transfected with 10 µg pNL4-3 plasmid DNA containing the WT sequence or indicated *pol* mutations within IN coding sequence. Two days post-transfection cell-free virions collected from cell culture supernatants were pelleted by ultracentrifugation through a 20% sucrose cushion using a Beckman SW41-Ti rotor at 28,000 rpm for 1.5 h at 4°C. Pelleted virions were resuspended in 1X PBS and treated with ethylene glycol bis(succinimidyl succinate) (EGS) (ThermoFisher Scientific), a membrane permeable crosslinker, at a concentration of 1 mM for 30 min at room temperature. Crosslinking was stopped by addition of SDS sample buffer. Samples were subsequently separated on 3-8% Tris-acetate gels and analyzed by immunoblotting using a mouse monoclonal anti-IN antibody [69].

Size exclusion chromatography (SEC)

All of the mutations were introduced into a plasmid backbone expressing His_6 tagged pNL4-3-derived IN by QuikChange site directed mutagenesis kit (Agilent) [60]. His_6 tagged recombinant pNL4-3 WT and mutant INs were expressed in BL21 (DE3) *E. coli* cells followed by nickel and heparin column purification as described previously [60, 73]. Recombinant WT and mutant INs were analyzed on Superdex 200 10/300 GL column (GE Healthcare) with running buffer containing 20 mM HEPES (pH 7.5), 1 M NaCl, 10% glycerol and 5 mM BME at 0.3 mL/min flow rate. The proteins were diluted to 10 µM with the running buffer and incubated for 1 h at 4°C followed by centrifugation at 10,000g for 10 min. Multimeric form determination was based on the standards including bovine thyroglobulin (670,000 Da), bovine gamma-globulin (158,000 Da), chicken ovalbumin (44,000 Da), horse myoglobin (17,000 Da) and vitamin B12 (1,350 Da).

Analysis of IN-RNA binding in vitro

Following SEC of IN as above, individual fractions of tetramer, dimer and monomer forms were collected and their binding to TAR RNA was analyzed by an Alpha screen assay as described previously [28]. Briefly, 100 nM His_6 tagged IN fractions (tetramer, dimer and monomer) were incubated with nickel acceptor beads while increasing concentrations of biotinylated-TAR RNA

was incubated with streptavidin donor beads in buffer containing 100 mM NaCl, 1 mM $MgCl_2$, 1 mM DTT, 1 mg/mL BSA, 25 mM Tris (pH 7.4). Followed by 2-h incubation at 4°C, they were mixed and the reading was taken after 1 h incubation at 4°C by PerkinElmer Life Sciences Enspire multimode plate reader. The Kd values were calculated using OriginLab software.

Virus production and transmission electron microscopy

Cell-free HIV-1 virions were isolated from transfected HEK293T cells. Briefly, cells grown in two 15-cm cell culture plates (10^7 cells per dish) were transfected with 30 μg full-length proviral plasmid (pNL4-3) DNA containing the WT sequence or indicated *pol* mutations within IN coding sequence using PolyJet DNA transfection reagent as recommended by the manufacturer (SignaGen Laboratories). Two days after transfection, cell culture supernatants were filtered through 0.22 μm filters and pelleted by ultracentrifugation using a Beckman SW32-Ti rotor at 26,000 rpm for 2 h at 4°C. Fixative (2.5% glutaraldehyde, 1.25% paraformaldehyde, 0.03% picric acid, 0.1 M sodium cacodylate, pH 7.4) was gently added to resulting pellets, and samples were incubated overnight at 4°C. The following steps were conducted at the Harvard Medical School Electron Microscopy core facility. Samples were washed with 0.1 M sodium cacodylate, pH 7.4 and postfixed with 1% osmium tetroxide /1.5% potassium ferrocyanide for 1 h, washed twice with water, once with maleate buffer (MB), and incubated in 1% uranyl acetate in MB for 1 h. Samples washed twice with water were dehydrated in ethanol by subsequent 10 minute incubations with 50%, 70%, 90%, and then twice with 100%. The samples were then placed in propyleneoxide for 1 h and infiltrated overnight in a 1:1 mixture of propyleneoxide and TAAB Epon (Marivac Canada Inc.). The following day the samples were embedded in TAAB Epon and polymerized at 60 °C for 48 h. Ultrathin sections (about 60 nm) were cut on a Reichert Ultracut-S microtome, transferred to copper grids stained with lead citrate, and examined in a JEOL 1200EX transmission electron microscope with images recorded on an AMT 2k CCD camera.

Images were captured at 30,000x magnification, and over 100 viral particles per sample were counted by visual inspection.

Equilibrium density sedimentation of virion core components in vitro

Equilibrium density sedimentation of virion core components was performed as previously described [64]. Briefly, HEK293T cells grown in 10-cm cell culture plates were transfected with 10 µg pNLGP plasmid DNA containing the WT sequence or indicated *pol* mutations within IN coding sequence. Two days post-transfection cell-free virions collected from cell culture supernatants were pelleted by ultracentrifugation through a 20% sucrose cushion using a Beckman SW41-Ti rotor at 28,000 rpm for 1.5 hr at 4°C. Pelleted viral-like particles were resuspended in PBS and treated with 0.5% Triton X-100 for 2 min at room temperature. Immediately after, samples were layered on top of 30-70% linear sucrose gradients prepared in 1X STE buffer (100 mM NaCl, 10 mM Tris-Cl (pH 8.0), 1 mM EDTA) and ultracentrifuged using a Beckman SW55-Ti rotor at 28,500 rpm for 16 h at 4°C. Fractions (500 µL) collected from the top of the gradients were analyzed for IN, CA, and MA by immunoblotting as detailed above.

Biochemical analysis of virion core components in infected cells

Biochemical analysis of retroviral cores in infected cells was performed as described previously [74]. Briefly, pgsA-745 cells were infected with VSV-G pseudotyped single cycle GFP-reporter viruses or its derivatives synchronously at 4°C. Following the removal of virus inoculum and extensive washes with PBS, cells were incubated at 37°C for 2 h. To prevent loss of vRNA due to reverse-transcription, cells were infected in the presence of 25 µM nevirapine. Post-nuclear supernatants were separated by ultracentrifugation on 10-50% linear sucrose gradients using a Beckman SW55-Ti rotor at 30,000 rpm for 1 h at 4°C. Ten 500 µl fractions from the top of the gradient were collected, and CA, IN, and vRNA in each fraction were analyzed by either immunoblotting or Q-PCR [74]. A SYBR-Green-based Q-PCR assay [70] was used to determine RT activity in the collected sucrose fractions.

Visualization of vRNA in infected cells

Viral RNA was visualized in infected cells according to the published multiplex immunofluorescent cell-based detection of DNA, RNA and Protein (MICDDRP) protocol [75]. VSV-G pseudotyped HIV-1_{NL4-3} virus stocks were prepared as described above and concentrated 40X using a lentivirus precipitation solution (ALSTEM). PgsA-745 cells were plated on 1.5 mm collagen-treated coverslips (GG-12-1.5-Collagen, Neuvitro) placed in 24-well plates one day prior to infection. Synchronized infections were performed by incubating pre-chilled virus inoculum on the cells for 30 min at 4°C. Cells were infected with WT virus at a MOI of 0.5, or with an equivalent number (normalized by RNA copy number) of IN mutant viral particles. After removal of the virus inoculum cells were washed with PBS and either immediately fixed with 4% paraformaldehyde, or incubated at 37°C for 2 h before fixing. To prevent loss of vRNA due to reverse-transcription, cells were infected and incubated in the presence of 25 μM nevirapine. Following fixation, cells were dehydrated with ethanol and stored at -20°C. Prior to probing for vRNA, cells were rehydrated, incubated in 0.1% Tween in PBS for 10 min, and mounted on slides. Probing was performed using RNAScope probes and reagents (Advanced Cell Diagnostics). Briefly, coverslips were treated with protease solution for 15 min in a humidified HybEZ oven (Advanced Cell Diagnostics) at 40 °C. The coverslips were then washed with PBS and pre-designed anti-sense probes [75] specific for HIV-1 vRNA were applied and allowed to hybridize with the samples in a humidified HybEZ oven at 40 °C for 2 h. The probes were visualized by hybridizing with preamplifiers, amplifiers, and finally, a fluorescent label. First, pre-amplifier 1 (Amp 1-FL) was hybridized to its cognate probe for 30 min in a humidified HybEZ oven at 40 °C. Samples were then subsequently incubated with Amp 2-FL, Amp 3-FL, and Amp 4A-FL for 15 min, 30 min, and 15 min respectively. Between adding amplifiers, the coverslips were washed with a proprietary wash buffer. Nuclei were stained with DAPI diluted in PBS at room temperature for 5 min. Finally, coverslips were washed in PBST followed by PBS and then mounted on slides using Prolong Gold Antifade.

Microscopy and image quantification

Images were taken using a Zeiss LSM 880 Airyscan confocal microscope equipped with a ×63/1.4 oil-immersion objective using the Airyscan super-resolution mode. 10 images were taken for each sample using the ×63 objective. Numbers of nuclei and vRNA punctae in images were counted using Volocity software (Quorum Technologies). The number of vRNA punctae per 100 nuclei were recorded at 0 h post-infection (hpi) and 2 hpi for each virus, and the number at 2 hpi compared to the number at 0 hpi.

Analysis of the fate of vRNA genome in MT4 cells

MT-4 cells were infected with VSV-G pseudotyped HIV-1 NL4-3 WT or equivalent number of mutant viruses (normalized by RT activity) synchronously at 4°C. After removal of virus inoculum and extensive washes with PBS, cells were incubated at 37°C for 6 h in the presence of 25 μM nevirapine. Immediately after synchronization (0 h) and at 2 and 6 h post-infection samples were taken from the infected cultures and RNA was isolated using TRIzol Reagent. The amount of viral genomic RNA was measured by Q-RT-PCR.

RESULTS

Characterization of the replication defects of class II IN mutant viruses

Substitutions in IN that exhibited a class II phenotype (i.e. assembly, maturation or reverse transcription defects [10-44, 76, 77] or affected IN multimerization [46, 78-81] were selected from past literature. The location of these substitutions depicted on the cryo-EM structure of the tetrameric HIV-1 intasome complex [9] indicate that many are positioned at or near monomer-monomer or dimer-dimer interfaces (Fig. 1A-B). While not apparent in the tetrameric intasome complex, the CTD mediates IN tetramer-tetramer interactions in the higher-order dodecamer IN structure [9] and has also been shown to mediate IN multimerization in vitro [15].

IN mutations were introduced into the replication competent pNL4-3 molecular clone and HEK293T cells were transfected with the resulting plasmids. Cell lysates and cell-free virions were subsequently analyzed for Gag/Gag-Pol expression, processing, particle release and infectivity. While substitutions in IN had no measurable effect on Gag (Pr55) expression, modest effects on Gag processing in cells was visible for several missense mutant viruses including H12N, N18I, K34A, Y99A, K103E, W108R, F185K, Q214L/Q216L, L242A, V260E, as well as the ΔIN mutant (Fig. 2A). Nevertheless, particle release was largely similar between WT and IN mutant viruses, as evident by the similar levels of CA protein present in cell culture supernatants (Fig. 2A, lower panels).

Three distinct phenotypes became apparent by assessing the amount of virion-associated IN and RT enzymes (Fig. 2A and Fig. S1A). First, virion-associated IN was at least 5-fold less than WT with several mutants, including H12N, N18I, K103E, W108R, F185K, L242A, and V260E (Fig. 2A and Table 1). Notably, these substitutions also reduced levels of Gag-Pol processing intermediates in producer cells (Fig. 2A) and RT in virions (Fig. 2A and Fig. S1A), suggesting that they likely destabilized the Gag-Pol precursor. Near complete lack of processing intermediates with the K14A and N18I substitutions, despite the presence of fully processed RT and IN in virions (detected using a separate polyclonal antibody), is likely due to inaccessibility of epitopes recognized by the monoclonal anti-IN antibody in the processing intermediates. Second, the R228A substitution abolished full-length IN in virions without impacting cell- or virion-associated Gag-Pol levels or processing intermediates; however, a faster migrating species due to altered charge in IN or that may represent product of aberrant IN processing and/or IN degradation was visible. A similar but more modest defect was observed for the K34A mutant, which was incorporated into virions at a modestly reduced level alongside a smaller protein species. Third, the remainder of the IN substitutions did not appear to affect IN or Gag-Pol levels in cells or virions.

With the exception of E96A, nearly all of the IN substitutions reduced virus titers at least 100-fold compared to the WT (Fig. 2B), which corresponded with reduced levels of reverse-transcription in infected cells (Fig. 2C). In line with previous reports [19, 20, 34], class II mutant IN molecules had variable levels of catalytic activity as assessed by the ability of Vpr-IN proteins to transcomplement a catalytically inactive IN (D116N, [11, 45]) in infected cells [68, 82]. All Vpr-IN fusion proteins, except for the H12N mutant which likely decreased the stability of the Vpr-IN fusion protein, were expressed at similar levels in cells (Fig. S1B). We found that K14A, E96A, Y99A, K103A, V165A, R187A, K188E R199A, K236E, and R269A/R273A IN mutants trans-complemented a catalytically inactive IN at levels similar to the WT, whereas W108R, R228A, and V260E mutants were unable to do so (Fig. 2D-E). The inability of W108R, R228A, and V260E mutants to transcomplement implies that they are impaired for integration, a result in line with previous observations [46, 81]. The remainder of the IN mutants restored integration, albeit at significantly lower than WT levels (Fig. 2D-E). These results suggest that the majority of the class II mutant INs retain structural integrity and at least partial catalytic activity in the presence of a complementing IN protein. Cumulatively, these data show that some class II substitutions in IN can affect the stability and/or processing of virion associated proteins, but they all universally lead to the formation of non-infectious virions that are blocked at reverse transcription in target cells, a hallmark of class II IN substitutions [10, 12].

Class II IN mutants abolish IN binding to RNA

Using complementary in vitro and CLIP-based approaches, we have previously shown that IN interacts with the viral genome through multiple basic residues (i.e. K264, K266, R269, K273) in its CTD [28]. In addition, IN-RNA interactions could also depend on proper IN multimerization, as ALLINI-induced aberrant IN multimerization potently inhibited the ability of IN to bind RNA [28]. Based on this, in the next set of experiments, we aimed to determine whether

379 class II IN mutants bind vRNA, and if not, whether improper IN multimerization may underlie this
380 defect.

381 IN-vRNA complexes were immunoprecipitated from UV-crosslinked virions and the
382 levels of coimmunoprecipitating vRNA was assessed. Note that substitutions that significantly
383 reduced the amount of IN in virions (Fig. 2A, Table 1) were excluded from these experiments.
384 All class II IN mutant viruses contained similar levels of vRNA, ruling out any inadvertent effects
385 of the alterations on RNA packaging (Fig. 3A). While the catalytically inactive IN D116N bound
386 vRNA at a level that was comparable to the WT, nearly all of the class II IN mutant proteins
387 failed to bind vRNA (Fig. 3B). The E96A substitution, which had a fairly modest effect on virus
388 titers as compared to other IN mutants (Fig. 2B), decreased but did not abolish the ability of IN
389 to bind RNA (Fig. 3B). Thus, lack of RNA binding ability is a surprisingly common property of a
390 disperse set of class II IN mutants, despite the fact that many of the altered amino acid residues
391 are distally located from the CTD.

392 **IN multimerization plays a key role in RNA binding**

393 As it seemed unlikely that all of the class II IN substitutions directly inhibited IN binding to
394 RNA, we reasoned that they might indirectly abolish binding by perturbing proper IN
395 multimerization. To test whether class II IN substitutions altered IN multimerization in a relevant
396 setting, purified HIV-1_{NL4-3} virions were treated with ethylene glycol bis (succinimidyl succinate)
397 (EGS) to covalently crosslink IN in situ and virus lysates were analyzed by immunoblotting. IN
398 species that migrated at molecular weights consistent with those of monomers, dimers, trimers
399 and tetramers were readily distinguished in WT virions (Fig. 4A). In the majority of the class II
400 mutant particles, IN appeared to be predominantly monomeric, with little dimers and no readily
401 detectable tetramers (Fig. 4A). In contrast to this general pattern, K34A, E96A, R262A/R263A
402 and R269A/K273A IN mutants formed dimers and tetramers at similar levels to the WT (Fig.

403 4A). An undefined smear was present at higher molecular weights for all virions, possibly as a
404 result of the formation of large IN aggregates upon cross-linking (Fig. 4A).

405 To corroborate these findings, we analyzed the multimerization properties of
406 recombinant WT, K34A, E96A, K188E, K236A and R262A/R263A IN proteins by SEC (Fig. 4B).
407 In line with the crosslinking studies in virions, WT, K34A and R262A/R263A IN molecules all
408 formed tetramers, while the levels of dimers varied between the mutants. For example, while IN
409 R262A/R263A presented similar levels of tetramers and dimers, IN K34A was primarily
410 tetrameric with a minor dimeric species, as evident by the broad right shoulder of the tetrameric
411 SEC peak (Fig. 4B). In contrast, E96A and K188E IN molecules almost exclusively formed
412 dimers and monomers with little evidence for tetramer formation (Fig. 4B). While K236E IN was
413 predominantly dimeric, the broad base of its chromatogram revealed some evidence for
414 tetramers and monomers as well (Fig. 4B).

415 We next determined the ability of IN monomers, dimers and tetramers to bind RNA to
416 test whether there is a causal link between the multimerization defects of class II IN
417 substitutions and RNA binding. Following size-exclusion chromatography (SEC)-based
418 separation of monomeric, dimeric and tetrameric IN, their affinity for TAR RNA, which
419 constitutes a high affinity binding site for IN [28], was assessed by an Alpha-screen assay.
420 Remarkably, while WT IN tetramers bound to TAR RNA at high affinity (2.68 ± 0.16 nM), neither
421 IN dimers nor monomers showed evidence of binding (Fig. 4C). Although IN K34A and IN
422 R262A/R263A could both form tetramers, IN K34A showed a reduced affinity for RNA while IN
423 R262A/R263A could not bind RNA at all (Fig. 4D).

424 Collectively, these results pointed to a key role of IN tetramerization in RNA binding and
425 suggest that a defect in proper multimerization underlies the inability of the majority of class II IN
426 mutants to bind vRNA. As the K34A and R262A/R263A substitutions did not affect IN

427 tetramerization, our findings suggest that these residues may be directly involved in IN binding
428 to RNA.

429 **Class II IN substitutions generate virions with eccentric morphology**

430 We next sought to determine how preclusion or inhibition of IN-vRNA interactions
431 correlated with particle morphology. Virion morphology of a subset of the IN mutants that
432 inhibited vRNA interactions by three different mechanisms; i.e. those that decreased IN levels in
433 virions (N18I and W108R), those that may have directly inhibited IN binding to RNA (K34A,
434 R262A/R263A), and those that primarily altered IN multimerization (E87A, E96A, F185K,
435 R187A, L241A, L242A), was assessed by transmission electron microscopy (TEM). As
436 expected, the majority of WT particles contained an electron dense condensate representing
437 vRNPs inside the CA lattice, whereas an ΔRT-IN deletion mutant virus produced similar levels
438 of immature particles and eccentric particles (Fig. 5A-B). Remarkably, irrespective of how IN-
439 RNA interactions were inhibited, 70-80% of nearly all class II IN mutant particles exhibited an
440 eccentric morphology (Fig. 5A-B). Of note, the E96A mutant tended to produce less eccentric
441 and more mature particles than the other IN mutants. Because IN E96A retained partial binding
442 to vRNA in virions (Fig. 3B) and partial infectivity (Fig. 2B), we conclude that this infection-
443 deferred mutant harbors a partial class II phenotype.

444 Next, we tested whether inhibition of IN-RNA interactions through class II substitutions
445 changes the localization of IN in virions. The premise for this is based on our previous finding
446 that disruption of IN binding to vRNA through the IN R269A/K273A substitution leads to
447 separation of a fraction of IN from dense vRNPs and CA containing complexes [64]. Thus, we
448 predicted that inhibition of IN-RNA interactions through the above class II substitutions could
449 lead to a similar outcome. To this end, WT or class II IN mutant virions stripped of the viral lipid
450 envelope by brief detergent treatment were separated on sucrose gradients, and resulting
451 fractions were analyzed for CA, IN, and matrix (MA) content by immunoblotting [64, 83]. As

before [64], WT IN migrated primarily in dense fractions, whereas the R269A/K273A mutant migrated bimodally (Fig. 6A, B). In contrast to our hypothesis, the majority of IN mutants sedimented similarly to WT IN and settled in the denser gradient fractions (Fig. 6A, B). Exceptions were the K34A and R262A/R263A IN mutants, a fraction of which migrated in soluble fractions similar to the R269A/K273A mutant, suggesting their localization outside of the capsid lattice. None of the IN substitutions affected the migration pattern of CA (Fig. 6C), which distributed bimodally between the soluble and dense fractions, nor the distribution of MA (data not shown), which was found in mainly the soluble fractions. These results suggested that, with the exception of the K34A, R262A/R263A, and R269A/K273A, IN mutant proteins may remain associated with the CA lattice despite inhibition of IN-vRNA interactions.

Premature loss of vRNA and IN from class II IN mutant viruses upon infection of target cells

We have previously shown that vRNA and IN are prematurely lost from cells infected with the R269A/K273A class II IN mutant [64]. Given that eccentric vRNP localization is a common feature of class II IN mutant viruses (Fig. 5), we next asked whether loss of vRNA in target cells is a common outcome for other class II IN mutant viruses. As the majority of mutant IN molecules appeared to remain associated with higher-order CA in virions (Fig. 6), we also wanted to test whether they would be protected from premature degradation in infected cells.

The fates of viral core components in target cells were tracked using a previously described biochemical assay [74]. For these experiments we utilized pgsA-745 cells (pgsA), which lack surface glycosaminoglycans, and likely as a result can be very efficiently infected by VSV-G-pseudotyped viruses in a synchronized fashion. PgsA cells were infected with WT or IN mutant viruses bearing substitutions that inhibited IN-vRNA interactions directly and led to mislocalization of IN in virions (i.e. K34A, R262A/R263A, R269A/K273A) or indirectly through aberrant IN multimerization and did not appear to grossly affect IN localization in virions (i.e.

E87A, V165A) (Fig 7A). Following infection, post-nuclear lysates were separated on linear sucrose gradients, and fractions collected from gradients were analyzed for viral proteins (CA, IN, RT) and vRNA by immunoblotting and Q-PCR-based assays, respectively.

As previously reported [64, 74], in cells infected with WT viruses, IN, RT, vRNA and a fraction of CA comigrated in sucrose fractions 6-8, representing active RTCs (Fig. 7B-E). Note that a large fraction of CA migrated in the top two soluble sucrose fractions representing CA that had dissociated from the core as a result of uncoating or CA that was packaged into virions but not incorporated into the capsid lattice [84, 85]. Notably, in cells infected with class II IN mutant viruses, equivalent levels of CA (Fig. 7B) and RT (Fig. 7D) remained in the denser fractions, whereas IN (Fig. 7C) and vRNA (Fig. 7E) were substantially reduced. Loss of vRNA and IN from dense fractions, without any corresponding increase in the top fractions containing soluble proteins and RNA, suggest their premature degradation and/or mislocalization in infected cells.

We next employed a complementary microcopy-based assay [75] in the context of full-length viruses to corroborate these findings. Advantages of this approach over biochemical fractionation experiments include the ability to track HIV-1 vRNA at the single-cell level with a high degree of specificity (Fig. S2A), determine its subcellular localization, and to side-step possible post-processing artifacts associated with biochemical fractionation. Cells were synchronously infected with VSV-G pseudotyped HIV-1_{NL4-3} in the presence of nevirapine to prevent vRNA loss due to reverse transcription, and vRNA levels associated with cells immediately following synchronization (0 h) and 2 h post-infection were evaluated [75]. In WT-infected cells, vRNA was clearly visible immediately after infection (Fig. 7F). Two h post infection, cell associated vRNA had fallen to 60-80% of starting levels (Fig. 7F, S2C), likely as the result of some viruses failing to enter or perhaps being degraded after entry. However, a significant proportion of vRNA was still readily detectable. In contrast, in cells infected with the IN mutant viruses the reduction in vRNA was greater, and by 2 h post-infection only 30-40% remained (Fig. 7F and Fig. S2B-C). These results support the conclusion from the biochemical

fractionation experiments that vRNA is prematurely lost from cells infected with class II IN mutant viruses.

Finally, we tested whether our findings held true in physiologically relevant human cells. MT-4 T cells were synchronously infected with WT or class II IN mutant VSV-G pseudotyped HIV-1_{NL4-3} in the presence of nevirapine. Cells were collected immediately after synchronization (0 h), 2 and 6 h post-infection, and the quantity of vRNA measured by Q-PCR. In line with the above findings, vRNA levels decreased at a faster rate with the class II IN mutants as compared to WT viruses, with half as much cell-associated vRNA remaining at 2 and 6 h post-infection for the class II IN mutants (Fig. 7G). Treating cells with ammonium chloride to prevent fusion of the VSV-G pseudotyped viruses rescued vRNA loss, and vRNA from WT and mutant viruses were retained at equal levels, indicating that the loss of vRNA is dependent on entry into the target cell (Fig. S2D). These findings agree with the previous experiments and demonstrate that class II IN substitutions lead to the premature loss of vRNA genome also in human T cells.

DISCUSSION

Our findings highlight the critical role of IN-vRNA interactions in virion morphogenesis and provide the mechanistic basis for how diverse class II IN substitutions lead to similar morphological and reverse transcription defects. We propose that class II IN substitutions lead to the formation of eccentric particles through three distinct mechanisms (Fig. 8): (i) depletion of IN from virions thus precluding the formation of IN-vRNA complexes; ii) impairment of functional IN multimerization and as a result, indirect disruption of IN-vRNA binding; iii) direct disruption of IN-vRNA binding without substantially affecting IN levels or its inherent multimerization properties. Irrespective of how IN binding to vRNA is inhibited, all substitutions led to the formation of eccentric viruses that were subsequently blocked at reverse transcription in target cells. We provide evidence that premature degradation of the exposed vRNPs and separation of RT from the vRNPs underlies the reverse transcription defect of class II IN mutants (Fig. 7).

Taken together, our findings cement the view that IN binding to RNA accounts for the role of IN in accurate particle maturation and provide the mechanistic basis of why these viruses are blocked at reverse transcription in target cells.

In regard to the first case (i) above, it was previously shown that IN deletion leads to the formation of eccentric particles [11, 27]. Thus, it is reasonable to assume that missense mutations that decreased IN levels in virions phenocopy IN deletion viruses. While it is also possible that these substitutions additionally affected IN binding to vRNA or multimerization, we could not reliably address these possibilities due to the extremely low levels of these proteins in virions.

Our results show the striking affinity of IN tetramers to bind RNA compared with IN monomers and dimers (Fig. 4C). In support of tetramerization being a prerequisite for RNA-binding, the inability of a number of class II IN mutant proteins to bind RNA was accompanied by a clear multimerization defect both in virions (Fig. 4A) and in vitro (Fig. 4B). The structural basis for IN binding to RNA is not yet known; however, these findings are in line with the previous in vitro evidence that hinted a link between IN multimerization and RNA-binding. For example, IN binds RNA as lower-order multimers, and conversely RNA binding may inhibit the formation of higher order IN multimers in vitro [28]. Notably, formation of open IN polymers that occlude the IN CTD from RNA binding may underlie the inhibition of IN-RNA interactions by ALLINIs [28, 58].

Based on MS-based footprinting experiments in vitro, we previously found that positively charged residues within the CTD of IN (i.e. K264, K266, K273) directly contact RNA, as was also validated by CLIP experiments [28]. Our findings here suggest that IN-vRNA contacts may extend to nearby basic residues within the CTD, such as R262 and R263, and perhaps more surprisingly, K34 within the IN NTD, as alterations of these residues did not prevent IN tetramerization (Fig. 4A-B) but completely abolished IN-vRNA binding in virions (Fig. 3B) and

553 reduced RNA-binding in vitro (Fig 4D). This raises the possibility of a second RNA-binding site
554 in the IN NTD. Structural analysis of IN in complex with RNA will be essential to definitively
555 determine how IN binds RNA as well as the precise multimeric species required for binding.

556 The mechanism by which IN-vRNA interactions mediate the encapsidation of vRNPs
557 inside the CA lattice remains unknown. One possibility is that the temporal coordination of
558 proteolytic cleavage events during maturation is influenced by IN-vRNA interactions [86, 87]. In
559 this scenario, the assembly of the CA lattice may become out of sync with the compaction of
560 vRNA by NC. Another possibility is that IN-vRNA complexes nucleate the assembly of the CA
561 lattice, perhaps by directly binding to CA. Notably, the biochemical assays performed herein
562 show that class II IN substitutions do not appear to affect the assembly and stability of the CA
563 lattice in vitro and in target cells. Although this finding is in disagreement with the previously
564 observed morphological aberrations of the CA lattice present in eccentric particles [26], it is
565 possible that the biochemical experiments used herein lack the level of sensitivity required to
566 quantitatively assess these aberrations. Further studies deciphering the crosstalk between IN-
567 RNA interactions and CA assembly will be critical to our understanding of the role of IN in
568 accurate virion maturation.

569 While the mislocalization of the vRNA genome in eccentric particles can be accurately
570 assessed by TEM analysis, precisely where IN is located in eccentric particles remains an open
571 question. Earlier studies based on biochemical separation of core components from detergent-
572 treated IN R269A/K273A virions indicated that IN may also mislocalize outside the CA lattice
573 [64]. In this study, only two class II IN mutants (K34A and R262A/R263A) revealed this
574 phenotype (Fig. 6A, B). It is intriguing that the bimodal distribution of IN in this experimental
575 setting was only seen with IN mutants that directly inhibited IN binding to vRNA. A possible
576 explanation for these observations is that improperly multimerized IN is retained within the CA
577 lattice or in association with it. Despite this co-migration pattern with CA, we found that both

578 E87A and V165A mutant INs were rapidly lost in infected cells, suggesting that they are not fully
579 protected by CA upon cellular entry (Fig. 7C).

580 Why is the unprotected vRNA and IN prematurely lost in target cells? It seems evident
581 that the protection afforded by the CA lattice matters the most for vRNP stability, though we
582 cannot rule out that IN binding to vRNA may in and of itself stabilize both the genome and IN.
583 Alternatively, the AU-rich nucleotide content of HIV-1 may destabilize its RNA [88-90], similar to
584 several cellular mRNAs that encode for cytokines and growth factors [91]. Finally, RNA nicking
585 and deadenylation in virions by virion associated enzymes [92-94] may predispose retroviral
586 genomes to degradation when they are prematurely exposed to the cytosolic milieu. While
587 cytosolic IN undergoes proteasomal degradation when expressed alone in cells [95-99], we
588 have found previously that proteasome inhibition does not rescue vRNA or IN in target cells
589 infected with a class II IN mutant [64]. Further studies are needed to determine whether a
590 specific cellular mechanism or an inherent instability of vRNPs is responsible from the loss of
591 vRNA in infected cells.

592 In conclusion, we have identified IN-vRNA binding as the underlying factor for the role of
593 IN in virion morphogenesis and show that virion morphogenesis is necessary to prevent the
594 premature loss of vRNA and IN early in the HIV-1 lifecycle. Despite relatively high barriers,
595 drugs that inhibit the catalytic activity of IN do select for resistance, and additional drug classes
596 that inhibit IN activity through novel mechanisms of action would be a valuable addition to
597 currently available treatments. The finding that IN-vRNA interaction can be inhibited in multiple
598 ways- by directly altering residues in the IN CTD or by altering IN multimerization in virions- can
599 help guide the design of future anti-retroviral compounds.

600

601 **FIGURE LEGENDS**

Figure 1. Class II IN substitutions locate throughout IN and cluster at interfaces that mediate IN multimerization.

(A) Location of class II IN substitutions used in this study displayed in red on a single IN monomer within the context of the HIV-1 IN tetramer intasome structure consisting of a dimer of dimers (PDB 5U1C). The two dimers are displayed in either gray or green, with individual monomers within each displayed in different shades. The DNA is omitted for clarity. (B) View of the structure displayed in A rotated 90°.

Figure 2. Characterization of the replication defects of class II IN mutant viruses.

(A) Immunoblot analysis of Gag and Gag-Pol products in cell lysates and virions. HEK293T cells were transfected with proviral HIV-1_{NL4-3} expression plasmids carrying *pol* mutations encoding for the indicated IN substitutions. Cell lysates and purified virions were harvested two days post transfection and analyzed by immunoblotting for CA, IN and, in the case of virions, RT. Representative image of one of four independent experiments is shown. (B) Infectious titers of WT or IN mutant HIV-1_{NL4-3} viruses in cell culture supernatants were determined on TZM-bl indicator cells. Titer values are expressed relative to WT (set to 1). Columns show average of five independent experiments (open circles) and error bars represent standard deviation (****P < 0.0001, by one-way ANOVA with Dunnett's multiple comparison test). (C) Relative quantity of reverse-transcribed HIV-1 DNA in MT-4 target cells infected with HIV-1_{NL4-3} at 6 hpi. Quantities of vDNA are expressed relative to WT (set to 1). Columns show average of three independent experiments (open circles) and error bars represent standard deviation (****P < 0.0001, by one-way ANOVA with Dunnett's multiple comparison test). (D) Representative growth curve of HIV-1_{NL4-3} IN_{D116N} viruses trans-complemented with class II mutant IN proteins in cell culture. Y-axis indicates fold increase in virion yield over day 0 as measured by RT activity in culture supernatants. HIV-1_{NL4-3} IN_{D116N} viruses that were trans-complemented with WT IN, class II

627 mutant INs, IN_{D116N}, or an empty vector are denoted as red, black, dark blue and light blue lines
628 respectively. Representative plot from one of three independent experiments. (E) Fold increase
629 in virions in culture supernatants at 4 dpi, as measured by RT activity in culture supernatants.
630 Trans-complementation of the HIV-1_{NL4-3} IN_{D116N} virus with mutant IN molecules restored particle
631 release to levels comparable to WT IN (red), partially restored particle release (gray) or could
632 not restore particle release (blue). Columns show average of three independent experiments
633 (open circles) and error bars represent standard deviation (*P < 0.05 and **P < 0.01, by paired t
634 test between individual mutants and WT).
635
636 **Figure 3. Class II IN substitutions prevent IN binding to the vRNA genome in virions.**
637 (A) Analysis of the levels of packaged viral genomic RNA in WT and IN mutant HIV-1_{NL4-3}
638 virions. vRNA extracted from purified virions was measured by Q-PCR. Data was normalized to
639 account for differences in particle yield using an RT activity assay. Normalized quantities of
640 vRNA are expressed relative to WT (set to 1). Columns show the average of three-four
641 independent experiments (open circles) and error bars represent standard deviation (ns, not
642 significant, by one-way ANOVA). (B) Representative autoradiogram of IN-RNA adducts
643 immunoprecipitated from WT or IN mutant HIV-1_{NL4-3} virions. The amount of immunoprecipitated
644 material was normalized such that equivalent levels of WT and mutant IN proteins were loaded
645 on the gel, as also evident in the immunoblots shown below. Levels of IN and CA in input virion
646 lysates is shown in the lower immunoblots. Data is representative of three independent
647 replicates.
648
649 **Figure 4. Multimerization properties of class II IN mutants.**
650 (A) Immunoblot analyses of IN multimers in virions. Purified WT or IN mutant HIV-1_{NL4-3} virions
651 were treated with 1 mM EGS, and virus lysates analyzed by immunoblotting using antibodies
652 against IN following separation on 6% Tris-acetate gels. Position of monomers (M), dimers (D),

and tetramers (T) are indicated by arrows. Representative image of one of three independent experiments is shown. (B) SEC profiles of 10 μM INs by Superdex 200 10/300 GL column. X-axis indicates elution volume (mL) and Y-axis indicate the intensity of absorbance (mAU). Tetramers (T), Dimers (D) and Monomers (M) are indicated. Representative chromatograms from two independent analyses are shown. (C) Analysis by Alpha screen assay of 100 nM WT IN monomers, dimers, and tetramers binding to biotinylated TAR RNA after separation by SEC. Graphed data is the average of three independent experiments and error bars indicate standard deviation. (D) Analysis of 100 nM WT or mutant INs binding to biotinylated TAR RNA by Alpha screen assay. Graphed data is the average of three independent experiments and error bars indicate standard deviation.

Figure 5. Analysis of class II IN mutant virion morphologies viruses by TEM.

(A) Representative TEM images of WT, K14A, N18I, K34A, E87A, E96A, W108R, F185K, R187A, L241A, L242A, R262A/R263A, and ΔRT-IN HIV-1_{NL4-3} virions. Magnification is 30,000x (scale bar, 100 nm). Black arrows indicate mature particles containing conical or round cores with associated electron density; triangles indicate eccentric particles with electron dense material situated between translucent cores and the viral membrane; diamonds indicate immature particles. (B) Quantification of virion morphologies. Columns show the average of two independent experiments (more than 100 particles counted per experiment) and error bars represent standard deviation.

Figure 6. Biochemical analysis of class II IN mutant virus particles.

(A) Immunoblot analysis of sedimentation profiles of IN in WT or IN mutant virions. Purified HIV-1_{NLGP} virions were analyzed by equilibrium density centrifugation as detailed in Materials and Methods. Ten fractions collected from the top of the gradients were analyzed by immunoblotting using antibodies against IN. Representative images from one of four independent experiments

679 are shown. (B) Quantitation of IN signal intensity in immunoblots as in (A) are shown. Profile of
680 WT virions is denoted in black, IN mutants that led to bimodal IN distribution are shown in red
681 and others are shown in grey. Graphed data is the average of two independent experiments and
682 error bars indicate the range. (C) Representative immunoblot analysis of sedimentation profile
683 of CA in WT virions and quantitation of CA signal intensity in immunoblots are shown. Profile of
684 WT virions is denoted in black, IN mutants that led to bimodal IN distribution are shown in red
685 and others are shown in grey. Graphed data is the average of two independent experiments and
686 error bars indicate the range.
687
688 **Figure 7. Premature loss of vRNA and IN from class II IN mutant viruses upon infection of**
689 **target cells.**

690 (A) Locations of the class II IN substitutions K34A, E87A, V165A and R262A/R263A displayed
691 on a single IN monomer within the context of the HIV-1 IN tetramer intasome structure (PDB
692 5U1C.) Substitutions are color coded based on whether they putatively caused mislocalization
693 of IN in virions (black) or not (blue.) (B-E) PgsA-745 cells were infected with WT or IN mutant
694 HIV-1 virions and fates of viral core components were analyzed 2 hpi. Fractions were analyzed
695 for the presence of CA (B) and IN (C) by immunoblotting and for RT activity (D) and vRNA (E)
696 by Q-PCR. Immunoblots are representative of three independent experiments. Graphed data in
697 (D) and (E) is the average of three independent experiments with error bars indicating standard
698 deviation (*P < 0.05 and **P < 0.01, by repeated measures one-way ANOVA.) (F)
699 Representative images of pgsA-745 cells infected with WT or IN mutant HIV-1_{NL4-3} viruses 0 and
700 2 hpi. Cells were stained for vRNA (green) and nuclei (blue) as detailed in Materials and
701 Methods. (G) Fraction of viral RNA remaining after 2 and 6 hpi compared to the quantity
702 measured at 0 hpi. MT-4 cells were synchronously infected with VSV-G pseudotyped HIV-1_{NL4-3}
703 viruses and at each timepoint samples of infected cultures were taken for analysis. Viral RNA

levels in samples were measured by Q-PCR and normalized to the levels of GAPDH mRNA. Data points are the average of five independent experiments with error bars indicating standard error of the mean.

Figure 8. Model depicting how class II IN mutants exert their effects on HIV-1 replication

Figure S1. Characterization of the replication defects of class II IN mutant viruses.

(A) Reverse-transcriptase activity measured in HIV-1_{NL4-3} virion lysates. For each repetition RT activities for the IN mutants are expressed relative to the WT (set to 1.) Columns show average of two independent experiments (open circles) and error bars represent standard deviation (****P < 0.0001, ***P < 0.001, **P < 0.01, and *P < 0.05, by unpaired t test between individual mutants and WT.) (B) Representative immunoblot analysis of Vpr-IN fusion constructs in cell lysates. HEK293T cells were co-transfected with the HIV-1_{NL4-3} IN_{D116N} proviral plasmid along with Vpr-IN expression plasmids encoding for the indicated IN substitutions or an empty vector control. Expression of Vpr-IN constructs in cell lysates was detected using an anti-IN antibody.

Figure S2. Premature loss of vRNA and IN from class II IN mutant viruses upon infection of target cells.

(A) Representative images of uninfected pgsA-745 cells and cells infected with WT HIV-1_{NL4-3} viruses at 0 hpi. Cells were fixed and stained for vRNA (green) and nuclei (blue). (B) Representative images of pgsA745 cells infected with IN mutant HIV-1_{NL4-3} viruses 0 and 2 hpi. Cells were fixed and stained for vRNA (green) and nuclei (blue). (C) Quantification of vRNA remaining in cells infected with WT or IN mutant HIV-1_{NL4-3} viruses at 2 hpi. Values are the percent of vRNA remaining at 2 hpi compared to at 0 hpi. Columns show average of three independent experiments (open circles) and error bars represent standard deviation (*P < 0.05 and **P < 0.01, by one-way ANOVA with Dunnett's multiple comparison test.) (D) Fraction of

729 viral RNA remaining after 2 and 6 hpi compared to the quantity measured at 0 hpi. MT-4 cells
730 were synchronously infected with VSV-G pseudotyped HIV-1_{NL4-3} viruses and incubated in the
731 presence of 50 mM ammonium chloride for 6 hrs. At each timepoint samples of infected cultures
732 were taken for analysis and levels of viral RNA in samples were measured by Q-PCR and
733 normalized to the levels of GAPDH mRNA. Data points are the average of three independent
734 experiments with error bars indicating standard error of the mean.
735

736 **ACKNOWLEDGEMENTS:** We thank Dr. Michael Malim for providing the anti-IN monoclonal
737 antibody and members of the Tolia lab for assisting in PyMol analysis. This study was supported
738 by grants NIH grants P50 GM103297 (the Center for HIV RNA Studies) and GM122458
739 to SBK, AI143389-F31 fellowship to JE, R01 AI062520 to MK and SBK, U54 AI150472 to MK
740 and AE, AI070042 to AE.
741
742 **REFERENCES**

743 1. Sundquist, W.I. and H.G. Krausslich, *HIV-1 assembly, budding, and maturation.* Cold
744 Spring Harb Perspect Med, 2012. **2**(7): p. a006924.
745 2. Pornillos, O. and B.K. Ganser-Pornillos, *Maturation of retroviruses.* Curr Opin Virol,
746 2019. **36**: p. 47-55.
747 3. Bieniasz, P. and A. Telesnitsky, *Multiple, Switchable Protein:RNA Interactions Regulate*
748 *Human Immunodeficiency Virus Type 1 Assembly.* Annu Rev Virol, 2018. **5**(1): p. 165-
749 183.
750 4. Engelman, A., *Reverse transcription and integration*, in *Retroviruses: Molecular Biology,*
751 *Genomics and Pathogenesis*, R. Kurth, Bannert, N., Editor. 2010, Caister Academic
752 Press: Norfolk, UK. p. 129-159.
753 5. Engelman, A.N., *Multifaceted HIV integrase functionalities and therapeutic strategies for*
754 *their inhibition.* J Biol Chem, 2019.
755 6. Lesbats, P., A.N. Engelman, and P. Cherepanov, *Retroviral DNA Integration.* Chem Rev,
756 2016. **116**(20): p. 12730-12757.
757 7. Engelman, A.N. and P. Cherepanov, *Retroviral intasomes arising.* Curr Opin Struct Biol,
758 2017. **47**: p. 23-29.
759 8. Ballandras-Colas, A., et al., *A supramolecular assembly mediates lentiviral DNA*
760 *integration.* Science, 2017. **355**(6320): p. 93-95.
761 9. Passos, D.O., et al., *Cryo-EM structures and atomic model of the HIV-1 strand transfer*
762 *complex intasome.* Science, 2017. **355**(6320): p. 89-92.
763 10. Engelman, A., *In vivo analysis of retroviral integrase structure and function.* Adv Virus
764 Res, 1999. **52**: p. 411-26.

11. Engelman, A., et al., *Multiple effects of mutations in human immunodeficiency virus type 1 integrase on viral replication.* J Virol, 1995. **69**(5): p. 2729-36.
12. Engelman, A., *The pleiotropic nature of human immunodeficiency virus integrase mutations.*, in *HIV-1 Integrase: Mechanism and Inhibitor Design* N. Neamati, Editor. 2011, John Wiley & Sons, Inc.: Hoboken, N.J. . p. 67-81.
13. Ansari-Lari, M.A., L.A. Donehower, and R.A. Gibbs, *Analysis of human immunodeficiency virus type 1 integrase mutants.* Virology, 1995. **213**(2): p. 680.
14. Bukovsky, A. and H. Gottlinger, *Lack of integrase can markedly affect human immunodeficiency virus type 1 particle production in the presence of an active viral protease.* J Virol, 1996. **70**(10): p. 6820-5.
15. Jenkins, T.M., et al., *A soluble active mutant of HIV-1 integrase: involvement of both the core and carboxyl-terminal domains in multimerization.* J Biol Chem, 1996. **271**(13): p. 7712-8.
16. Kalpana, G.V., et al., *Isolation and characterization of an oligomerization-negative mutant of HIV-1 integrase.* Virology, 1999. **259**(2): p. 274-85.
17. Leavitt, A.D., et al., *Human immunodeficiency virus type 1 integrase mutants retain in vitro integrase activity yet fail to integrate viral DNA efficiently during infection.* J Virol, 1996. **70**(2): p. 721-8.
18. Liao, W.H. and C.T. Wang, *Characterization of human immunodeficiency virus type 1 Pr160 gag-pol mutants with truncations downstream of the protease domain.* Virology, 2004. **329**(1): p. 180-8.
19. Lu, R., H.Z. Ghory, and A. Engelman, *Genetic analyses of conserved residues in the carboxyl-terminal domain of human immunodeficiency virus type 1 integrase.* J Virol, 2005. **79**(16): p. 10356-68.
20. Lu, R., et al., *Class II integrase mutants with changes in putative nuclear localization signals are primarily blocked at a postnuclear entry step of human immunodeficiency virus type 1 replication.* J Virol, 2004. **78**(23): p. 12735-46.
21. Nakamura, T., et al., *Lack of infectivity of HIV-1 integrase zinc finger-like domain mutant with morphologically normal maturation.* Biochem Biophys Res Commun, 1997. **239**(3): p. 715-22.
22. Quillent, C., et al., *Extensive regions of pol are required for efficient human immunodeficiency virus polyprotein processing and particle maturation.* Virology, 1996. **219**(1): p. 29-36.
23. Shin, C.G., et al., *Genetic analysis of the human immunodeficiency virus type 1 integrase protein.* J Virol, 1994. **68**(3): p. 1633-42.
24. Taddeo, B., W.A. Haseltine, and C.M. Farnet, *Integrase mutants of human immunodeficiency virus type 1 with a specific defect in integration.* J Virol, 1994. **68**(12): p. 8401-5.
25. Wu, X., et al., *Human immunodeficiency virus type 1 integrase protein promotes reverse transcription through specific interactions with the nucleoprotein reverse transcription complex.* J Virol, 1999. **73**(3): p. 2126-35.
26. Fontana, J., et al., *Distribution and Redistribution of HIV-1 Nucleocapsid Protein in Immature, Mature, and Integrase-Inhibited Virions: a Role for Integrase in Maturation.* J Virol, 2015. **89**(19): p. 9765-80.
27. Jurado, K.A., et al., *Allosteric integrase inhibitor potency is determined through the inhibition of HIV-1 particle maturation.* Proc Natl Acad Sci U S A, 2013. **110**(21): p. 8690-5.
28. Kessl, J.J., et al., *HIV-1 Integrase Binds the Viral RNA Genome and Is Essential during Virion Morphogenesis.* Cell, 2016. **166**(5): p. 1257-1268 e12.

29. Ao, Z., et al., *Contribution of the C-terminal tri-lysine regions of human immunodeficiency virus type 1 integrase for efficient reverse transcription and viral DNA nuclear import.* Retrovirology, 2005. **2**: p. 62.
30. Busschots, K., et al., *Identification of the LEDGF/p75 binding site in HIV-1 integrase.* J Mol Biol, 2007. **365**(5): p. 1480-92.
31. Engelman, A., et al., *Structure-based mutagenesis of the catalytic domain of human immunodeficiency virus type 1 integrase.* J Virol, 1997. **71**(5): p. 3507-14.
32. Limon, A., et al., *Nuclear localization of human immunodeficiency virus type 1 preintegration complexes (PICs): V165A and R166A are pleiotropic integrase mutants primarily defective for integration, not PIC nuclear import.* J Virol, 2002. **76**(21): p. 10598-607.
33. Lloyd, A.G., et al., *Characterization of HIV-1 integrase N-terminal mutant viruses.* Virology, 2007. **360**(1): p. 129-35.
34. Lu, R., et al., *Lys-34, dispensable for integrase catalysis, is required for preintegration complex function and human immunodeficiency virus type 1 replication.* J Virol, 2005. **79**(19): p. 12584-91.
35. Masuda, T., et al., *Genetic analysis of human immunodeficiency virus type 1 integrase and the U3 att site: unusual phenotype of mutants in the zinc finger-like domain.* J Virol, 1995. **69**(11): p. 6687-96.
36. Rahman, S., et al., *Structure-based mutagenesis of the integrase-LEDGF/p75 interface uncouples a strict correlation between in vitro protein binding and HIV-1 fitness.* Virology, 2007. **357**(1): p. 79-90.
37. Riviere, L., J.L. Darlix, and A. Cimarelli, *Analysis of the viral elements required in the nuclear import of HIV-1 DNA.* J Virol, 2010. **84**(2): p. 729-39.
38. Tsurutani, N., et al., *Identification of critical amino acid residues in human immunodeficiency virus type 1 IN required for efficient proviral DNA formation at steps prior to integration in dividing and nondividing cells.* J Virol, 2000. **74**(10): p. 4795-806.
39. Wiskerchen, M. and M.A. Muesing, *Human immunodeficiency virus type 1 integrase: effects of mutations on viral ability to integrate, direct viral gene expression from unintegrated viral DNA templates, and sustain viral propagation in primary cells.* J Virol, 1995. **69**(1): p. 376-86.
40. Zhu, K., C. Dobard, and S.A. Chow, *Requirement for integrase during reverse transcription of human immunodeficiency virus type 1 and the effect of cysteine mutations of integrase on its interactions with reverse transcriptase.* J Virol, 2004. **78**(10): p. 5045-55.
41. De Houwer, S., et al., *The HIV-1 integrase mutant R263A/K264A is 2-fold defective for TRN-SR2 binding and viral nuclear import.* J Biol Chem, 2014. **289**(36): p. 25351-61.
42. Johnson, B.C., et al., *A homology model of HIV-1 integrase and analysis of mutations designed to test the model.* J Mol Biol, 2013. **425**(12): p. 2133-46.
43. Mohammed, K.D., M.B. Topper, and M.A. Muesing, *Sequential deletion of the integrase (Gag-Pol) carboxyl terminus reveals distinct phenotypic classes of defective HIV-1.* J Virol, 2011. **85**(10): p. 4654-66.
44. Shehu-Xhilaga, M., et al., *The conformation of the mature dimeric human immunodeficiency virus type 1 RNA genome requires packaging of pol protein.* J Virol, 2002. **76**(9): p. 4331-40.
45. Engelman, A. and R. Craigie, *Identification of conserved amino acid residues critical for human immunodeficiency virus type 1 integrase function in vitro.* J Virol, 1992. **66**(11): p. 6361-9.
46. Lutzke, R.A. and R.H. Plasterk, *Structure-based mutational analysis of the C-terminal DNA-binding domain of human immunodeficiency virus type 1 integrase: critical residues for protein oligomerization and DNA binding.* J Virol, 1998. **72**(6): p. 4841-8.

47. Lutzke, R.A., C. Vink, and R.H. Plasterk, *Characterization of the minimal DNA-binding domain of the HIV integrase protein.* Nucleic Acids Res, 1994. **22**(20): p. 4125-31.
48. Balakrishnan, M., et al., *Non-catalytic site HIV-1 integrase inhibitors disrupt core maturation and induce a reverse transcription block in target cells.* PLoS One, 2013. **8**(9): p. e74163.
49. Sharma, A., et al., *A new class of multimerization selective inhibitors of HIV-1 integrase.* PLoS Pathog, 2014. **10**(5): p. e1004171.
50. Le Rouzic, E., et al., *Dual inhibition of HIV-1 replication by integrase-LEDGF allosteric inhibitors is predominant at the post-integration stage.* Retrovirology, 2013. **10**: p. 144.
51. Desimmie, B.A., et al., *LEDGINs inhibit late stage HIV-1 replication by modulating integrase multimerization in the virions.* Retrovirology, 2013. **10**: p. 57.
52. Slaughter, A., et al., *The mechanism of H171T resistance reveals the importance of Ndelta-protonated His171 for the binding of allosteric inhibitor BI-D to HIV-1 integrase.* Retrovirology, 2014. **11**: p. 100.
53. Amadori, C., et al., *The HIV-1 integrase-LEDGF allosteric inhibitor MUT-A: resistance profile, impairment of virus maturation and infectivity but without influence on RNA packaging or virus immunoreactivity.* Retrovirology, 2017. **14**(1): p. 50.
54. Gupta, K., et al., *Allosteric inhibition of human immunodeficiency virus integrase: late block during viral replication and abnormal multimerization involving specific protein domains.* J Biol Chem, 2014. **289**(30): p. 20477-88.
55. Bonnard, D., et al., *Structure-function analyses unravel distinct effects of allosteric inhibitors of HIV-1 integrase on viral maturation and integration.* J Biol Chem, 2018. **293**(16): p. 6172-6186.
56. Deng, N., et al., *Allosteric HIV-1 Integrase Inhibitors Promote Aberrant Protein Multimerization by Directly Mediating Inter-Subunit Interactions: Structural and Thermodynamic Modeling Studies.* Protein Sci, 2016.
57. Feng, L., et al., *The A128T resistance mutation reveals aberrant protein multimerization as the primary mechanism of action of allosteric HIV-1 integrase inhibitors.* J Biol Chem, 2013. **288**(22): p. 15813-20.
58. Gupta, K., et al., *Structural Basis for Inhibitor-Induced Aggregation of HIV Integrase.* PLoS Biol, 2016. **14**(12): p. e1002584.
59. Koneru, P.C., et al., *HIV-1 integrase tetramers are the antiviral target of pyridine-based allosteric integrase inhibitors.* Elife, 2019. **8**.
60. Kessl, J.J., et al., *Multimode, cooperative mechanism of action of allosteric HIV-1 integrase inhibitors.* J Biol Chem, 2012. **287**(20): p. 16801-11.
61. Engelman, A. and P. Cherepanov, *Retroviral Integrase Structure and DNA Recombination Mechanism.* Microbiol Spectr, 2014. **2**(6).
62. Tekeste, S.S., et al., *Interaction between Reverse Transcriptase and Integrase Is Required for Reverse Transcription during HIV-1 Replication.* J Virol, 2015. **89**(23): p. 12058-69.
63. van Bel, N., et al., *The allosteric HIV-1 integrase inhibitor BI-D affects virion maturation but does not influence packaging of a functional RNA genome.* PLoS One, 2014. **9**(7): p. e103552.
64. Madison, M.K., et al., *Allosteric HIV-1 Integrase Inhibitors Lead to Premature Degradation of the Viral RNA Genome and Integrase in Target Cells.* J Virol, 2017. **91**(17).
65. Zennou, V., et al., *APOBEC3G incorporation into human immunodeficiency virus type 1 particles.* J Virol, 2004. **78**(21): p. 12058-61.
66. Cowan, S., et al., *Cellular inhibitors with Fv1-like activity restrict human and simian immunodeficiency virus tropism.* Proc Natl Acad Sci U S A, 2002. **99**(18): p. 11914-9.

67. Hatziioannou, T., et al., *Restriction of multiple divergent retroviruses by Lv1 and Ref1.* EMBO J, 2003. **22**(3): p. 385-94.
68. Liu, H., et al., *Incorporation of functional human immunodeficiency virus type 1 integrase into virions independent of the Gag-Pol precursor protein.* J Virol, 1997. **71**(10): p. 7704-10.
69. Bouyac-Bertoia, M., et al., *HIV-1 infection requires a functional integrase NLS.* Mol Cell, 2001. **7**(5): p. 1025-35.
70. Pizzato, M., et al., *A one-step SYBR Green I-based product-enhanced reverse transcriptase assay for the quantitation of retroviruses in cell culture supernatants.* J Virol Methods, 2009. **156**(1-2): p. 1-7.
71. Kutluay, S.B., et al., *Global changes in the RNA binding specificity of HIV-1 gag regulate virion genesis.* Cell, 2014. **159**(5): p. 1096-109.
72. Kutluay, S.B. and P.D. Bieniasz, *Analysis of HIV-1 Gag-RNA Interactions in Cells and Virions by CLIP-seq.* Methods Mol Biol, 2016. **1354**: p. 119-31.
73. Cherepanov, P., *LEDGF/p75 interacts with divergent lentiviral integrases and modulates their enzymatic activity in vitro.* Nucleic Acids Res, 2007. **35**(1): p. 113-24.
74. Kutluay, S.B., D. Perez-Caballero, and P.D. Bieniasz, *Fates of retroviral core components during unrestricted and TRIM5-restricted infection.* PLoS Pathog, 2013. **9**(3): p. e1003214.
75. Puray-Chavez, M., et al., *Multiplex single-cell visualization of nucleic acids and protein during HIV infection.* Nat Commun, 2017. **8**(1): p. 1882.
76. Englund, G., et al., *Integration is required for productive infection of monocyte-derived macrophages by human immunodeficiency virus type 1.* J Virol, 1995. **69**(5): p. 3216-9.
77. Petit, C., O. Schwartz, and F. Mammano, *Oligomerization within virions and subcellular localization of human immunodeficiency virus type 1 integrase.* J Virol, 1999. **73**(6): p. 5079-88.
78. Eijkelenboom, A.P., et al., *Refined solution structure of the C-terminal DNA-binding domain of human immunovirus-1 integrase.* Proteins, 1999. **36**(4): p. 556-64.
79. Hare, S., et al., *Structural basis for functional tetramerization of lentiviral integrase.* PLoS Pathog, 2009. **5**(7): p. e1000515.
80. Kessl, J.J., et al., *An allosteric mechanism for inhibiting HIV-1 integrase with a small molecule.* Mol Pharmacol, 2009. **76**(4): p. 824-32.
81. Li, X., Y. Koh, and A. Engelman, *Correlation of recombinant integrase activity and functional preintegration complex formation during acute infection by replication-defective integrase mutant human immunodeficiency virus.* J Virol, 2012. **86**(7): p. 3861-79.
82. Fletcher, T.M., 3rd, et al., *Complementation of integrase function in HIV-1 virions.* EMBO J, 1997. **16**(16): p. 5123-38.
83. Welker, R., et al., *Biochemical and structural analysis of isolated mature cores of human immunodeficiency virus type 1.* J Virol, 2000. **74**(3): p. 1168-77.
84. Briggs, J.A., et al., *The stoichiometry of Gag protein in HIV-1.* Nat Struct Mol Biol, 2004. **11**(7): p. 672-5.
85. Ganser-Pornillos, B.K., A. Cheng, and M. Yeager, *Structure of full-length HIV-1 CA: a model for the mature capsid lattice.* Cell, 2007. **131**(1): p. 70-9.
86. Konnyu, B., et al., *Gag-Pol processing during HIV-1 virion maturation: a systems biology approach.* PLoS Comput Biol, 2013. **9**(6): p. e1003103.
87. Pettit, S.C., et al., *Ordered processing of the human immunodeficiency virus type 1 GagPol precursor is influenced by the context of the embedded viral protease.* J Virol, 2005. **79**(16): p. 10601-7.

88. Maldarelli, F., M.A. Martin, and K. Strebel, *Identification of posttranscriptionally active inhibitory sequences in human immunodeficiency virus type 1 RNA: novel level of gene regulation.* J Virol, 1991. **65**(11): p. 5732-43.
89. Schwartz, S., et al., *Mutational inactivation of an inhibitory sequence in human immunodeficiency virus type 1 results in Rev-independent gag expression.* J Virol, 1992. **66**(12): p. 7176-82.
90. Schwartz, S., B.K. Felber, and G.N. Pavlakis, *Distinct RNA sequences in the gag region of human immunodeficiency virus type 1 decrease RNA stability and inhibit expression in the absence of Rev protein.* J Virol, 1992. **66**(1): p. 150-9.
91. Wu, X. and G. Brewer, *The regulation of mRNA stability in mammalian cells: 2.0.* Gene, 2012. **500**(1): p. 10-21.
92. Gorelick, R.J., et al., *Characterization of the block in replication of nucleocapsid protein zinc finger mutants from moloney murine leukemia virus.* J Virol, 1999. **73**(10): p. 8185-95.
93. Miyazaki, Y., et al., *An RNA structural switch regulates diploid genome packaging by Moloney murine leukemia virus.* J Mol Biol, 2010. **396**(1): p. 141-52.
94. Sakuragi, J., T. Shioda, and A.T. Panganiban, *Duplication of the primary encapsidation and dimer linkage region of human immunodeficiency virus type 1 RNA results in the appearance of monomeric RNA in virions.* J Virol, 2001. **75**(6): p. 2557-65.
95. Mulder, L.C. and M.A. Muesing, *Degradation of HIV-1 integrase by the N-end rule pathway.* J Biol Chem, 2000. **275**(38): p. 29749-53.
96. Ali, H., et al., *Cellular TRIM33 restrains HIV-1 infection by targeting viral integrase for proteasomal degradation.* Nat Commun, 2019. **10**(1): p. 926.
97. Llano, M., et al., *Lens epithelium-derived growth factor/p75 prevents proteasomal degradation of HIV-1 integrase.* J Biol Chem, 2004. **279**(53): p. 55570-7.
98. Zheng, Y., et al., *Host protein Ku70 binds and protects HIV-1 integrase from proteasomal degradation and is required for HIV replication.* J Biol Chem, 2011. **286**(20): p. 17722-35.
99. Devroe, E., A. Engelman, and P.A. Silver, *Intracellular transport of human immunodeficiency virus type 1 integrase.* J Cell Sci, 2003. **116**(Pt 21): p. 4401-8.

A

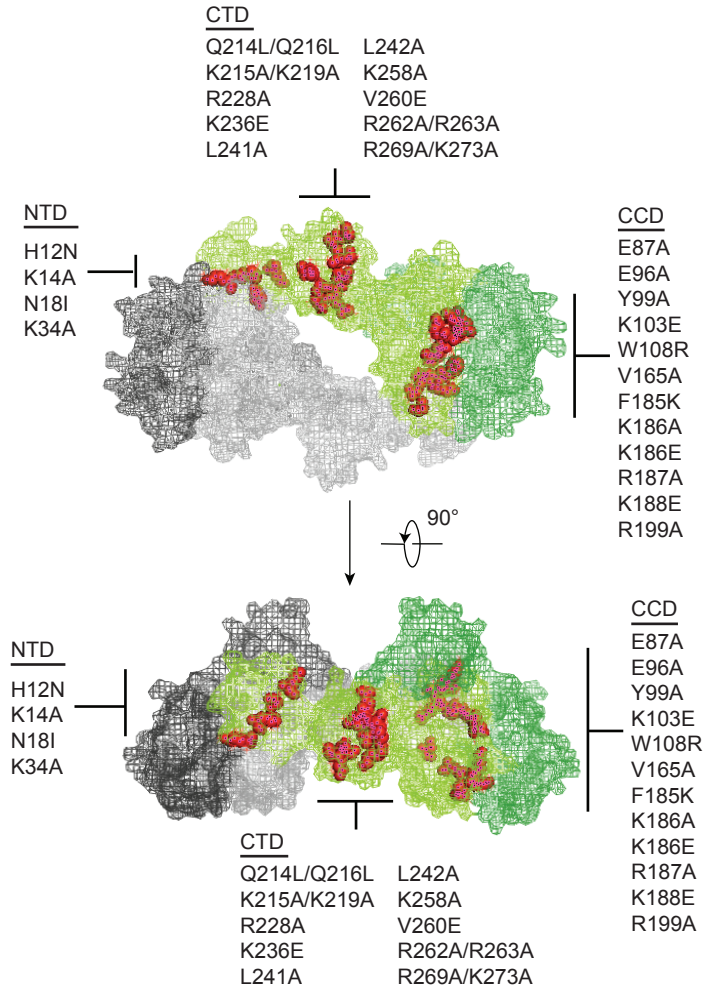
CTD
Q214L/Q216L
K215A/K219A
R228A
K236E
L241A
L242A
K258A
V260E
R262A/R263A
R269A/K273A
NTD
H12N
K14A
N18I
K34A
CCD
E87A
E96A
Y99A
K103E
W108R
V165A
F185K
K186A
K186E
R187A
K188E
R199A
90°

B

NTD
H12N
K14A
N18I
K34A
CCD
E87A
E96A
Y99A
K103E
W108R
V165A
F185K
K186A
K186E
R187A
K188E
R199A
CTD
Q214L/Q216L
K215A/K219A
R228A
K236E
L241A
L242A
K258A
V260E
R262A/R263A
R269A/K273A

Figure 1

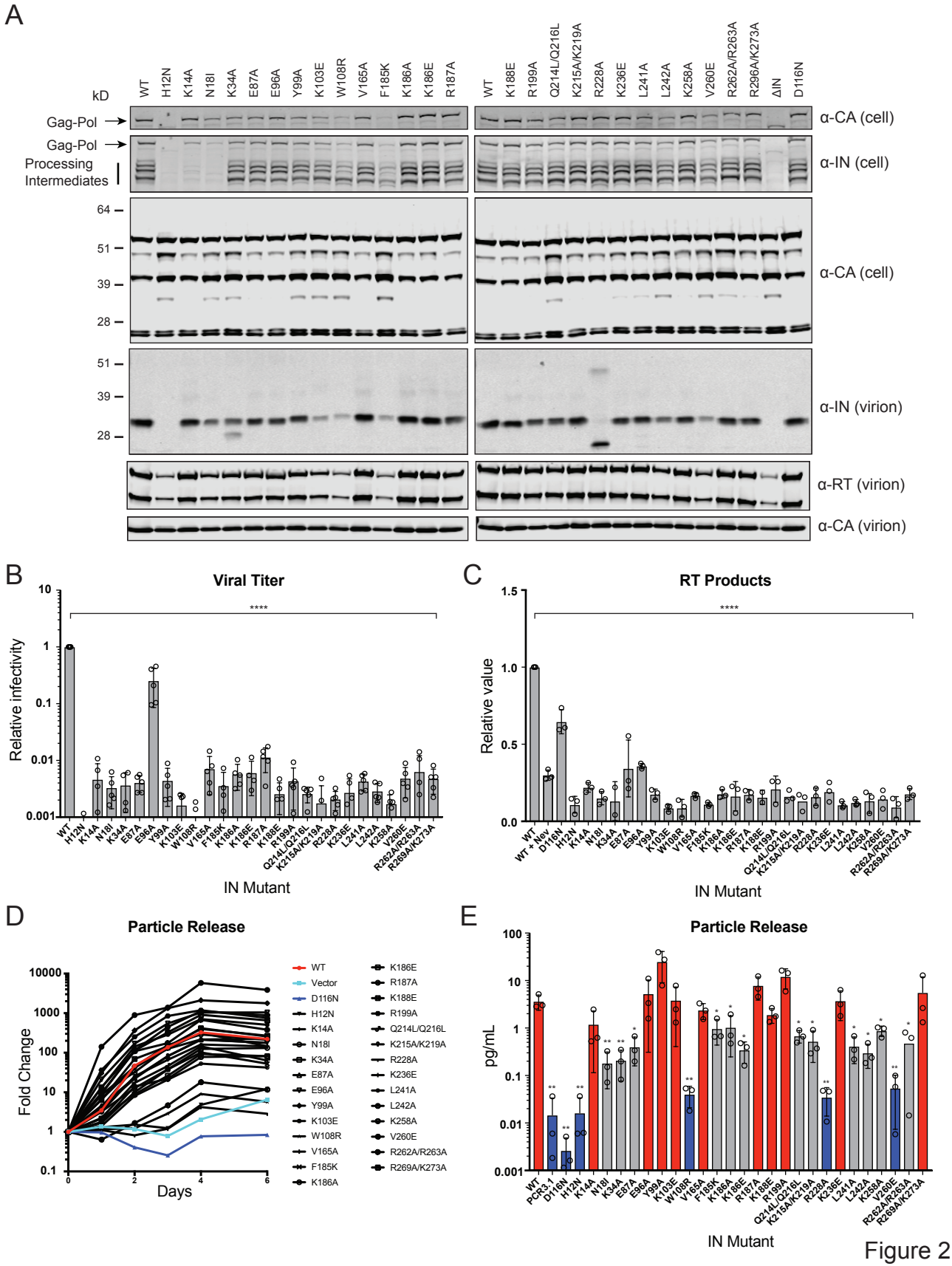
A
kD
WT
H12N
K14A
N18I
K34A
E87A
E96A
Y99A
K103E
W108R
V165A
F185K
K186A
K186E
R187A
WT
K188E
R199A
Q214L/Q216L
K215A/K219A
R228A
K236E
L241A
L242A
K258A
V260E
R262A/R263A
R296A/K273A
ΔIN
D116N
Gag-Pol
Gag-Pol
Processing
Intermediates
64
51
39
28
51
39
28
α-CA (cell)
α-IN (cell)
α-CA (cell)
α-IN (virion)
α-RT (virion)
α-CA (virion)
B
Viral Titer
Relative infectivity
10
1
0.1
0.01
0.001
****
WT
H12N
K14A
N18I
K34A
E87A
E96A
Y99A
K103E
W108R
V165A
F185K
K186A
K186E
R187A
K188E
R199A
Q214L/Q216L
K215A/K219A
R228A
K236E
L241A
L242A
K258A
V260E
R262A/R263A
R269A/K273A
IN Mutant
C
RT Products
Relative value
1.5
1.0
0.5
0.0
****
WT
WT + Nev
D116N
H12N
K14A
N18I
K34A
E87A
E96A
Y99A
K103E
W108R
V165A
F185K
K186A
K186E
R187A
K188E
R199A
Q214L/Q216L
K215A/K219A
R228A
K236E
L241A
L242A
K258A
V260E
R262A/R263A
R269A/K273A
IN Mutant
D
Particle Release
Fold Change
10000
1000
100
10
1
0.1
0
2
4
6
Days
WT
Vector
D116N
H12N
K14A
N18I
K34A
E87A
E96A
Y99A
K103E
W108R
V165A
F185K
K186A
K186E
R187A
K188E
R199A
Q214L/Q216L
K215A/K219A
R228A
K236E
L241A
L242A
K258A
V260E
R262A/R263A
R269A/K273A
E
Particle Release
pg/mL
100
10
1
0.1
0.01
0.001
WT
PCR3.1
D116N
H12N
K14A
N18I
K34A
E87A
E96A
Y99A
K103E
W108R
V165A
F185K
K186A
K186E
R187A
K188E
R199A
Q214L/Q216L
K215A/K219A
R228A
K236E
L241A
L242A
K258A
V260E
R262A/R263A
R269A/K273A
IN Mutant

Figure 2

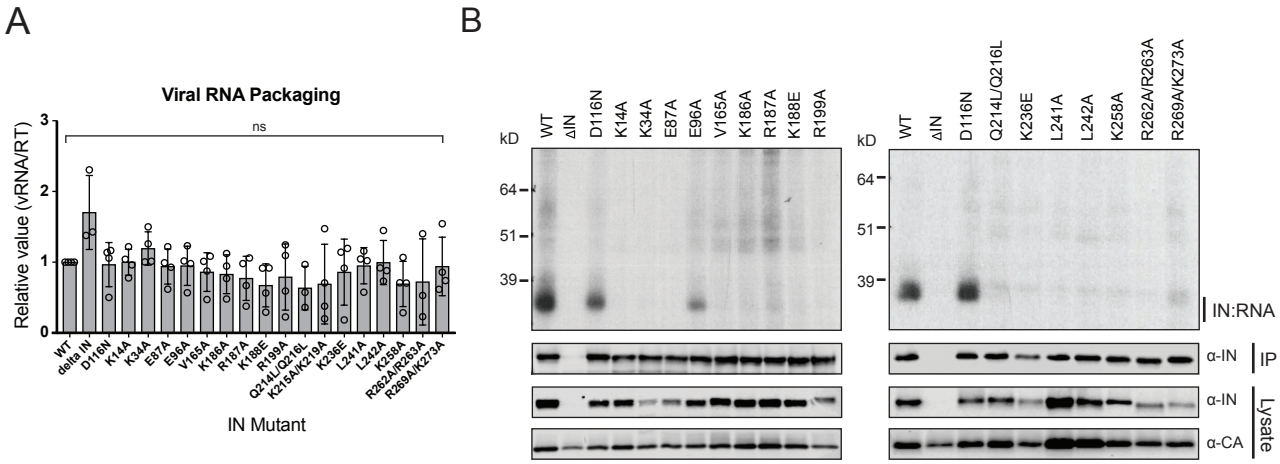
A
Viral RNA Packaging
ns
Relative value (vRNA/RT)
3
2
1
0
WT
delta IN
D116N
K14A
K34A
E87A
E96A
V165A
K186A
R187A
K188E
R199A
Q214L/Q216L
K215A/K219A
K236E
L241A
L242A
K258A
R262A/R263A
R269A/K273A
IN Mutant
B
kD
WT
ΔIN
D116N
K14A
K34A
E87A
E96A
V165A
K186A
R187A
K188E
R199A
64
51
39
kD
WT
ΔIN
D116N
Q214L/Q216L
K236E
L241A
L242A
K258A
R262A/R263A
R269A/K273A
64
51
39
IN:RNA
α-IN
IP
α-IN
Lysate
α-CA

Figure 3

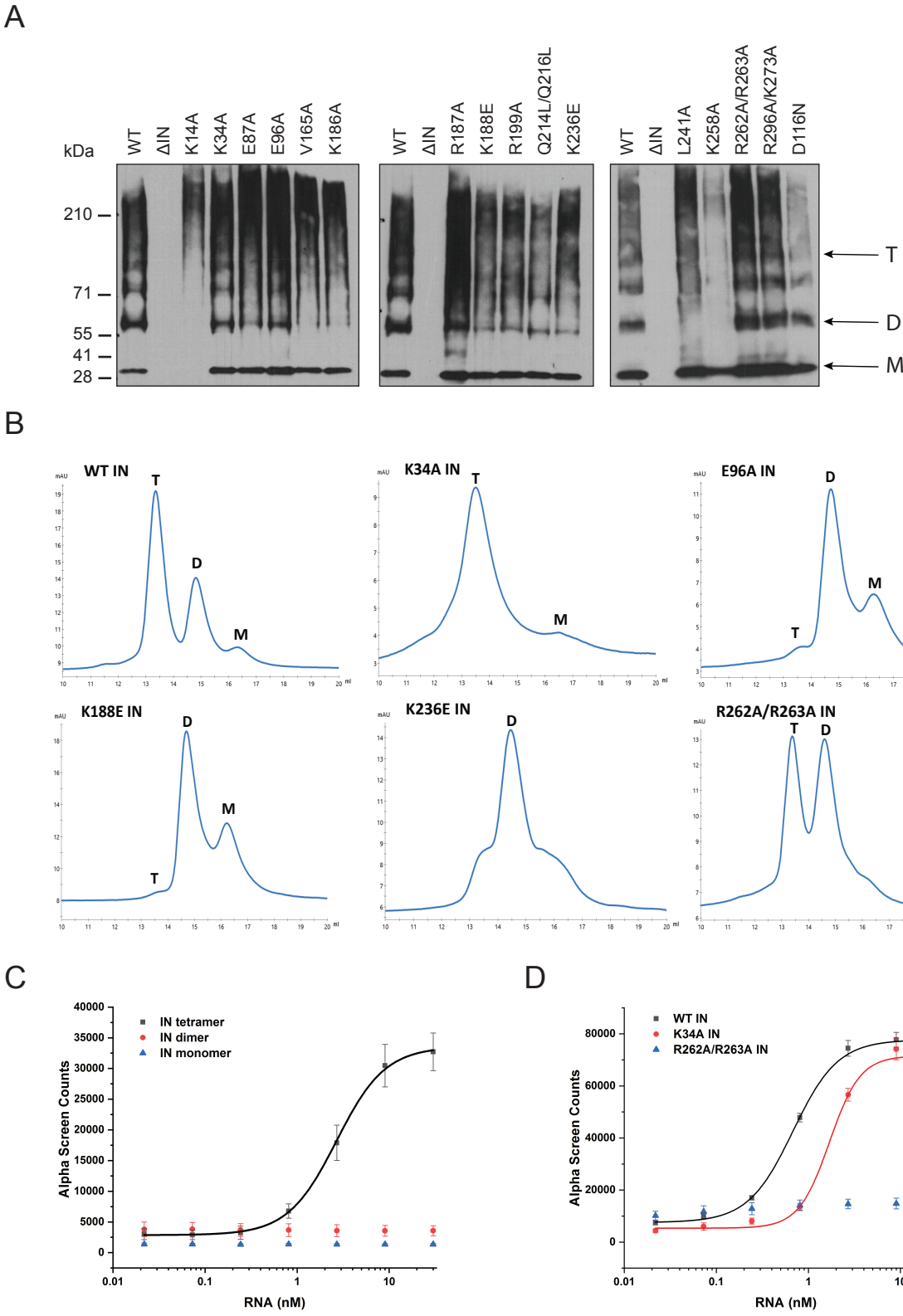
A
kDa
WT
ΔIN
K14A
K34A
E87A
E96A
V165A
K186A
R187A
K188E
R199A
Q214L/Q216L
K236E
L241A
K258A
R262A/R263A
R296A/K273A
D116N
210
71
55
41
28
T
D
M
B
WT IN
K34A IN
E96A IN
K188E IN
K236E IN
R262A/R263A IN
C
IN tetramer
IN dimer
IN monomer
Alpha Screen Counts
RNA (nM)
D
WT IN
K34A IN
R262A/R263A IN
Alpha Screen Counts
RNA (nM)

Figure 4

A

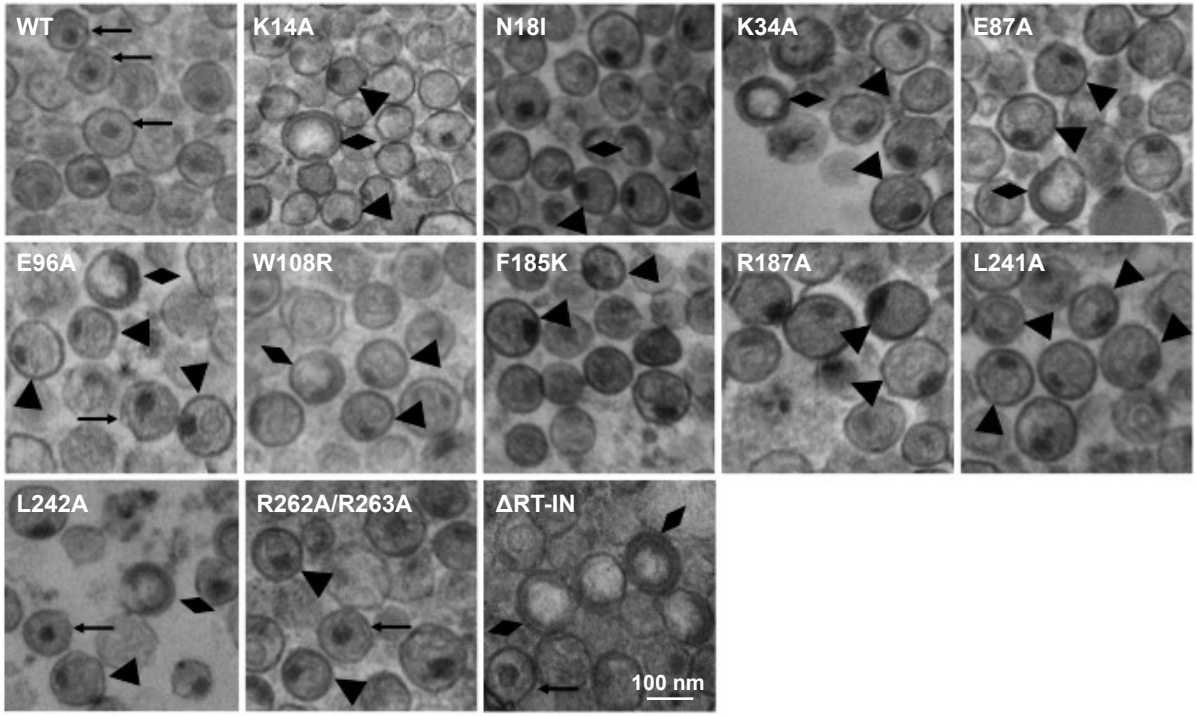
WT
K14A
N18I
K34A
E87A
E96A
W108R
F185K
R187A
L241A
L242A
R262A/R263A
ΔRT-IN
100 nm

B

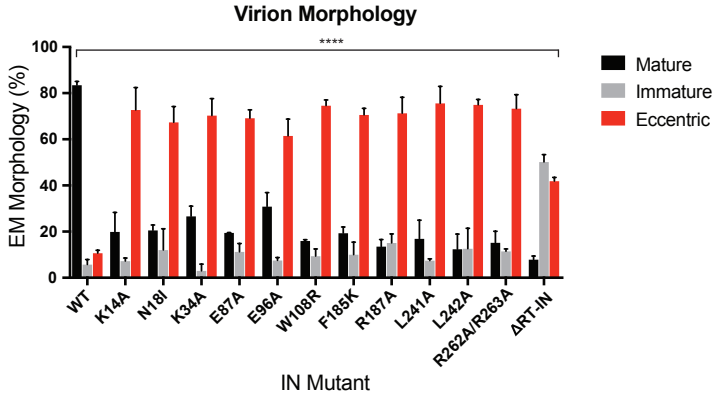
Virion Morphology
****
EM Morphology (%)
100
80
60
40
20
0
WT
K14A
N18I
K34A
E87A
E96A
W108R
F185K
R187A
L241A
L242A
R262A/R263A
ΔRT-IN
IN Mutant
Mature
Immature
Eccentric

Figure 5

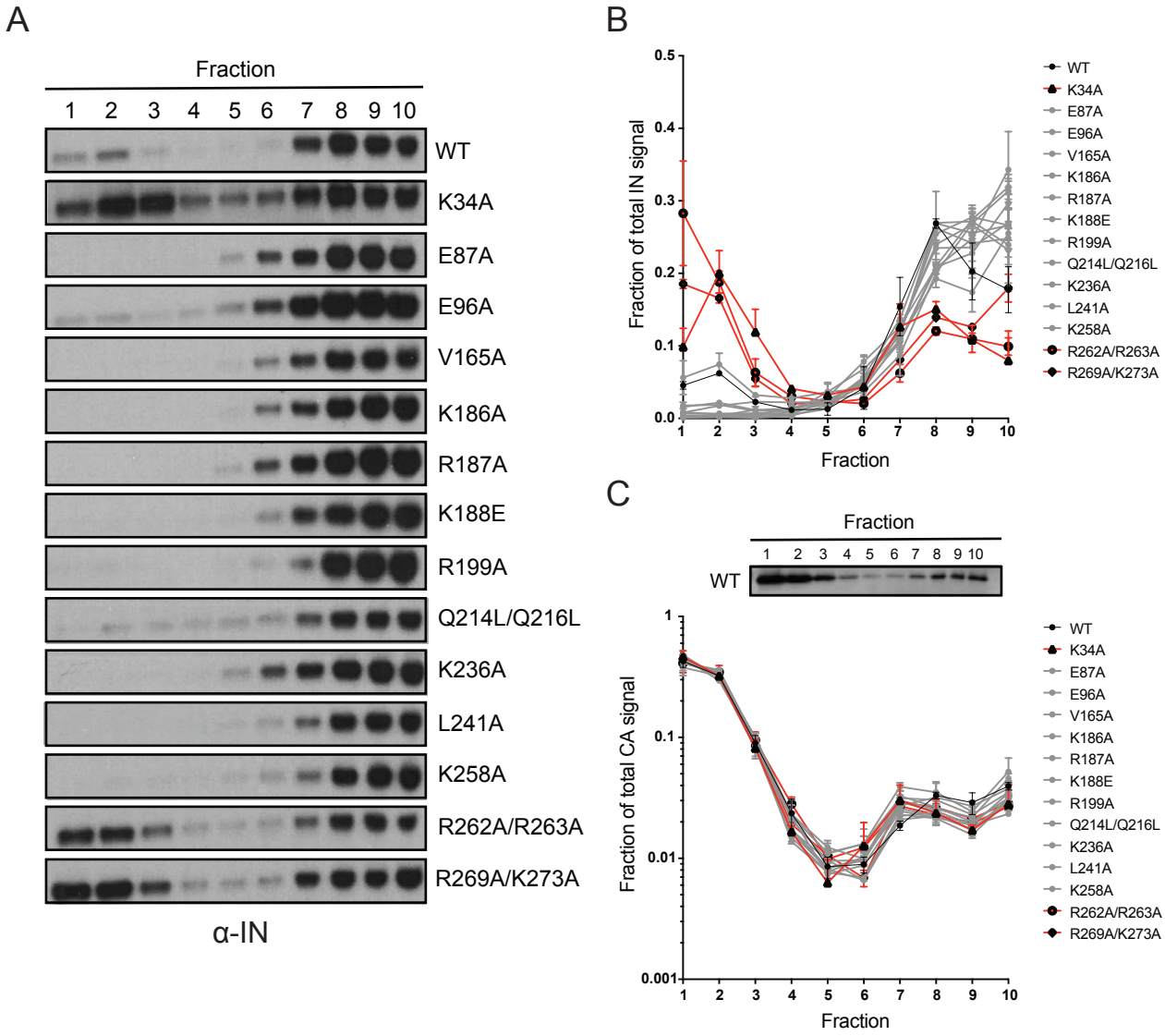
A
Fraction
1 2 3 4 5 6 7 8 9 10
WT
K34A
E87A
E96A
V165A
K186A
R187A
K188E
R199A
Q214L/Q216L
K236A
L241A
K258A
R262A/R263A
R269A/K273A
α-IN
B
Fraction of total IN signal
Fraction
C
Fraction
WT
Fraction of total CA signal
Fraction

Figure 6

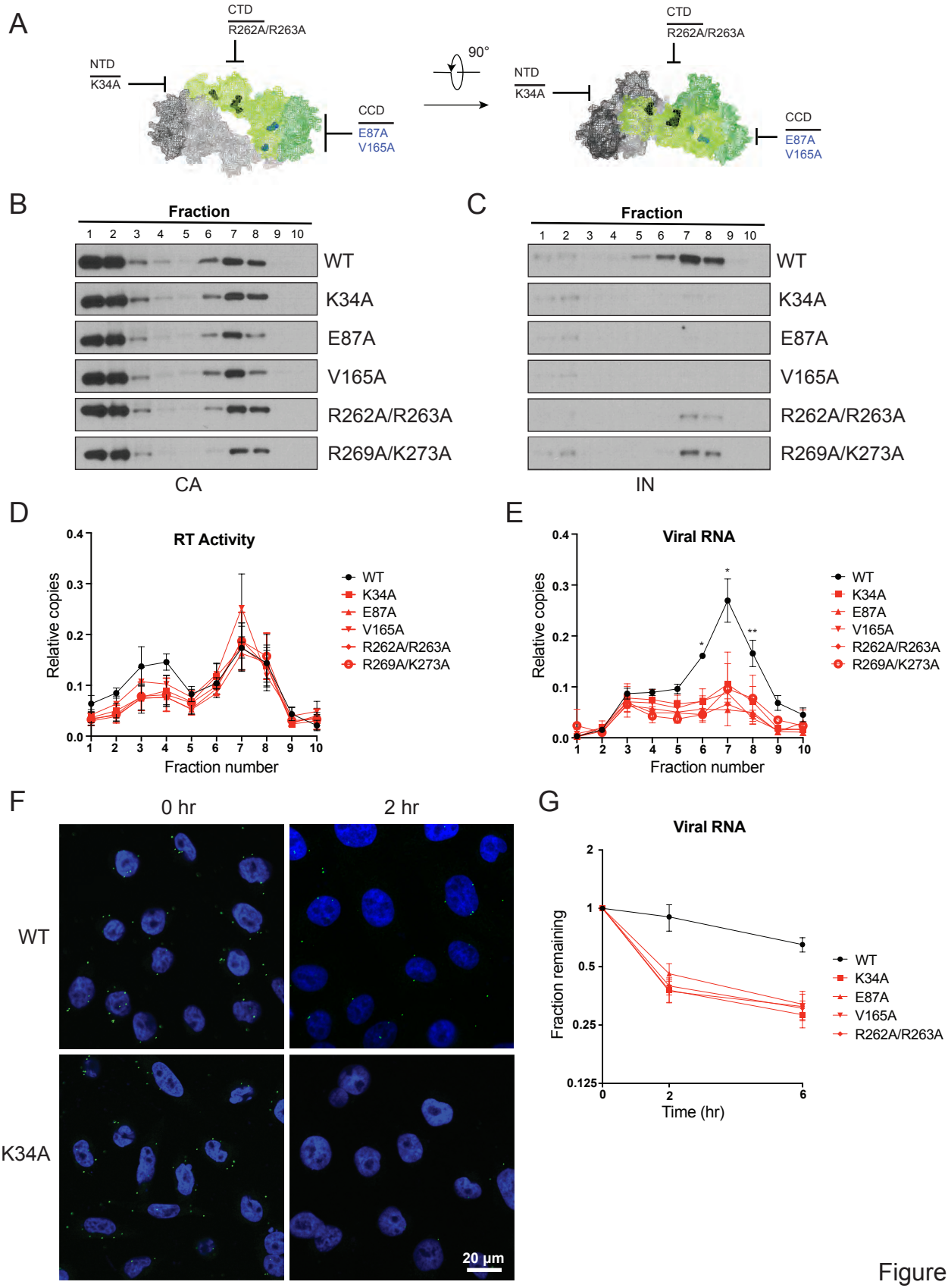
A
CTD
R262A/R263A
NTD
K34A
CCD
E87A
V165A
90°
B
Fraction
1 2 3 4 5 6 7 8 9 10
WT
K34A
E87A
V165A
R262A/R263A
R269A/K273A
CA
C
IN
D
RT Activity
Relative copies
Fraction number
E
Viral RNA
F
0 hr
2 hr
WT
K34A
20 µm
G
Fraction remaining
Time (hr)

Figure 7

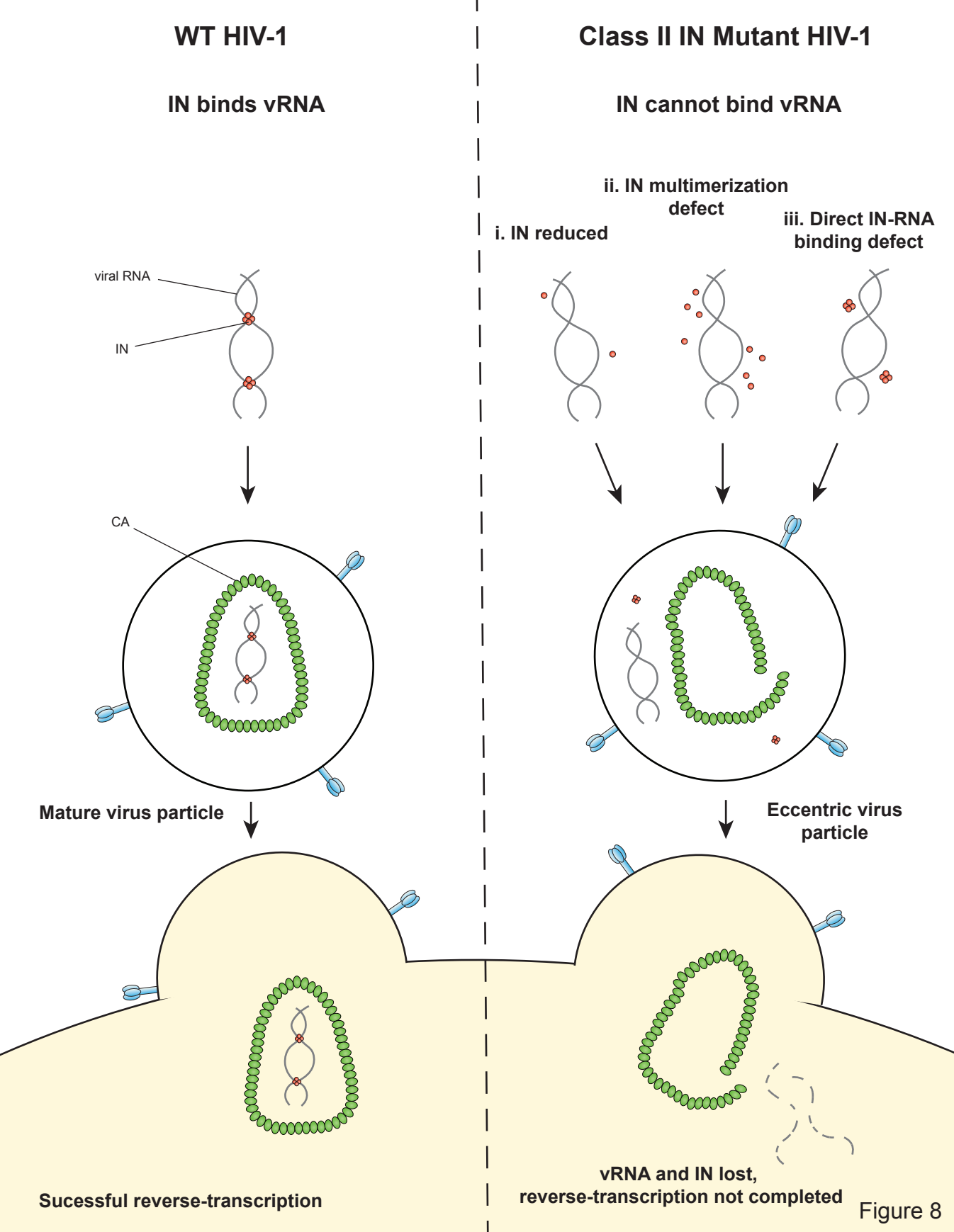
WT HIV-1
IN binds vRNA
Class II IN Mutant HIV-1
IN cannot bind vRNA
ii. IN multimerization defect
i. IN reduced
iii. Direct IN-RNA binding defect
viral RNA
IN
CA
Mature virus particle
Eccentric virus particle
Sucessful reverse-transcription
vRNA and IN lost, reverse-transcription not completed

Figure 8

Table 1: IN levels in virions

IN mutant	IN signal (%)	SD	IN mutant	IN signal (%)	SD
WT	100	N/A	K186E	63.2	16.4
H12N	ND	N/A	R187A	34.4	24.5
K14A	40.5	10.3	K188E	45.8	26.3
N18I	16.7	3.1	R199A	41.1	19.2
K34A	32.6	6.9	Q214L/Q216L	31.7	6.3
E87A	31.4	16.1	K215A/K219A	47.7	20.4
E96A	38.4	31.2	R228A	50.2	26.4
Y99A	22.0	10.3	K236E	37.4	14.0
K103E	6.8	2.3	L241A	41.4	12.4
W108R	2.7	0.3	L242A	13.7	3.5
V165A	55.6	32.8	K258A	36.7	19.7
F185K	2.5	1.6	V260E	6.0	4.0
K186A	69.4	27.9	R262A/R263A	52.9	7.0

Quantitation of IN in virions as measured by immunoblotting. For each experiment IN signal was normalized to CA signal for each virus, and the resulting value compared to that of WT (set at 100%.) Reported values are the average value (as percent of WT) and standard deviation (SD) between 4 independent experiments. Mutants with less than 20% IN signal of WT are highlighted in gray.

A

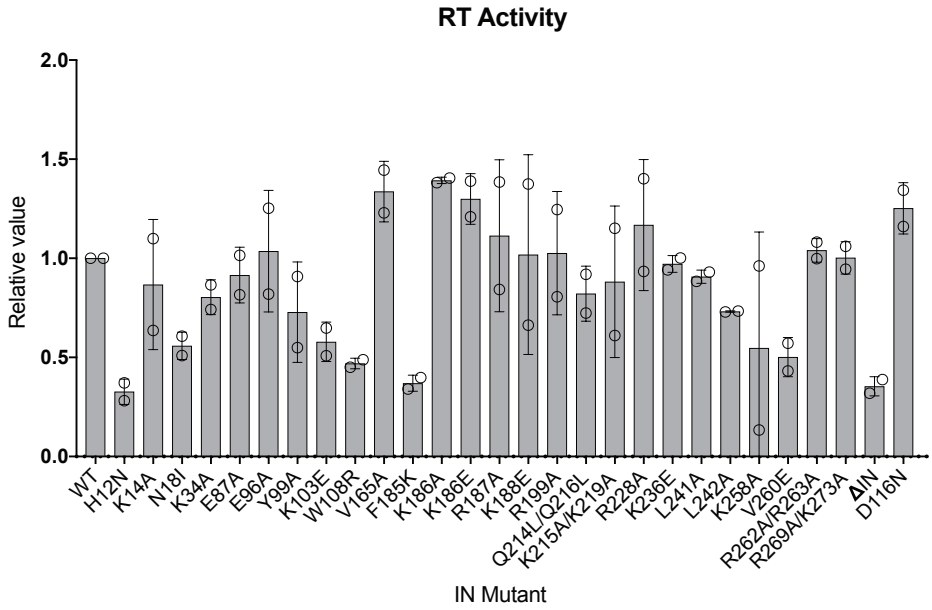
RT Activity
Relative value
2.0
1.5
1.0
0.5
0.0
WT
H12N
K14A
N18I
K34A
E87A
E96A
Y99A
K103E
W108R
V165A
F185K
K186A
K186E
R187A
K188E
R199A
Q214L/Q216L
K215A/K219A
R228A
K236E
L241A
L242A
K258A
V260E
R262A/R263A
R269A/K273A
ΔIN
D116N
IN Mutant

B

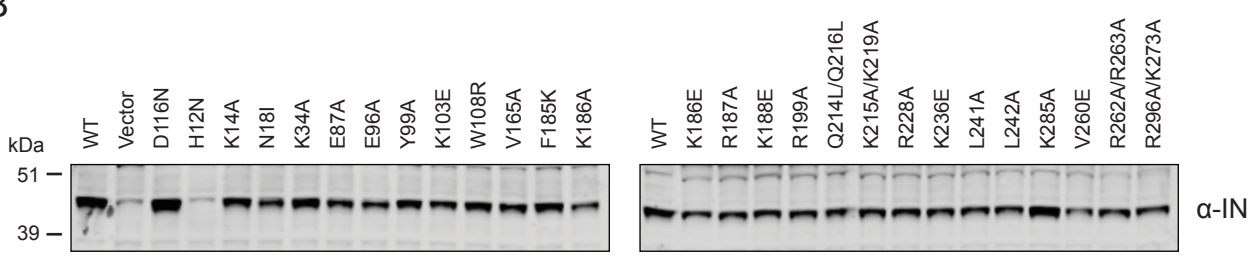
kDa
51
39
WT
Vector
D116N
H12N
K14A
N18I
K34A
E87A
E96A
Y99A
K103E
W108R
V165A
F185K
K186A
WT
K186E
R187A
K188E
R199A
Q214L/Q216L
K215A/K219A
R228A
K236E
L241A
L242A
K285A
V260E
R262A/R263A
R296A/K273A
α-IN

Figure S1

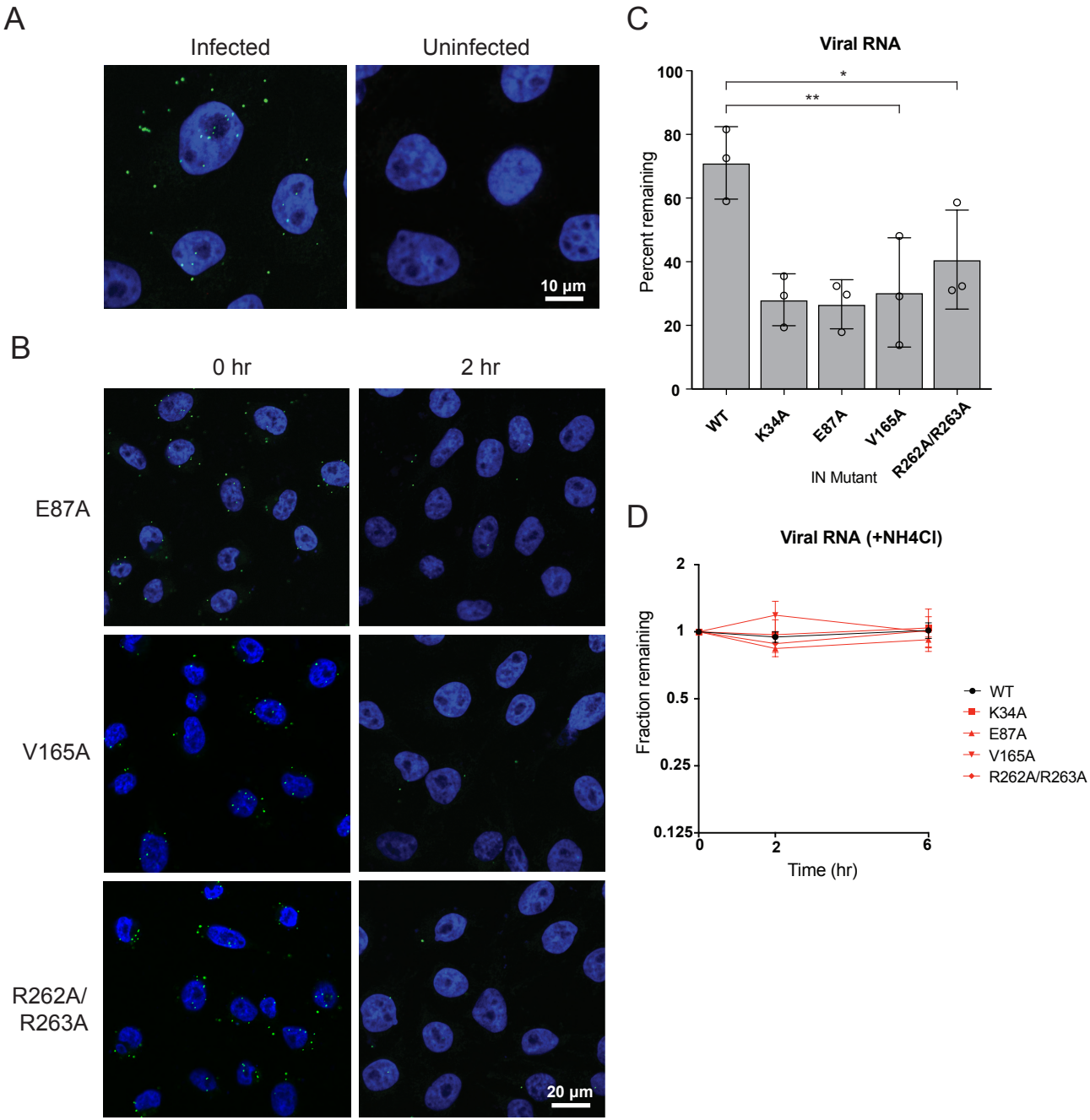
A
Infected
Uninfected
10 µm
B
0 hr
2 hr
E87A
V165A
R262A/
R263A
20 µm
C
Viral RNA
Percent remaining
100
80
60
40
20
0
*
**
WT
K34A
E87A
V165A
R262A/R263A
IN Mutant
D
Viral RNA (+NH4Cl)
Fraction remaining
2
1
0.5
0.25
0.125
0
2
6
Time (hr)
WT
K34A
E87A
V165A
R262A/R263A

Figure S2